FCC SAR Analysis Report

EnteroMedics Inc.

Model 200 Maestro Rechargeable System

FCC ID: 2ABHRMC2402

Submitted to

Scott Lambert, Director of Engineering
EnteroMedics Inc.
2800 Patton Road
St. Paul, MN 55113
651-634-3206
slambert@enteromedics.com

Prepared by

John Ross, Ph.D., P.E.
John Ross & Associates, LLC
3282 E. Vallejo Circle
Moab, Utah 84532
Voice: 801-359-5957
Fax: 801-931-2020

Report ENT-FCC-2015-03

March 29, 2015

PROPRIETARY AND CONFIDENTIAL

Table of Contents

1 Purpose....1
1.1 Revisions....1
1.2 Scope....1
1.3 System Overview....2
1.4 System Operation....4
1.4.1 Charging Procedure....4
1.4.2 Inductive System Description....4
2 SAR Analysis Overview....5
2.1 Software and Computer Tools....5
2.2 CAD Modeling....5
2.3 Material Properties and Tissue Modeling....8
2.4 Cell Size versus Memory and Run-time Requirements....9
2.5 Source Modeling Approach....11
3 Laboratory Measurements....12
3.1 Purpose....12
3.2 Equipment Used....12
3.3 B-Field Probe Conversion Formula....13
3.4 Test Configurations....13
3.5 B-Field Probe Locations....14
3.6 Centered Configuration Results....17
3.7 Offset Configuration....23
4 Spice Simulation and Source Modeling....29
4.1 Centered Configuration Analysis....29
4.1.1 TC coil current derivation....29
4.1.2 Current probe , voltage probe and cable delay corrections....29
4.1.3 Calculations and measurements....30
4.1.4 Kirchhoff's Law simulation....30
4.1.5 RNR coil current phase....31
4.1.6 Centered Configuration Source Condition Summary....32
4.2 Offset Configuration Analysis....32
4.2.1 TC coil current derivation....32
4.2.2 Current probe , voltage probe and cable delay corrections....32
4.2.3 Calculations and Measurements....32
4.2.4 Kirchhoff's Law simulation....33
4.2.5 RNR coil current phase....34
4.2.6 Offset Configuration Source Condition Summary....35
5 Field Simulation and Validation....36
5.1 Centered Configuration....36
5.1.1 Simulation Diagnostics....38
5.1.2 Computed Current and Voltage Waveforms....38
5.1.3 Computed B-fields....40
5.1.4 Additional H-Field and E-Field plots....42

5.1.5 Computed Power Dissipation Density....45
5.2 Offset Configuration....46
5.2.1 Simulation Diagnostics....47
5.2.2 Computed Current and Voltage Waveforms....47
5.2.3 Computed B-fields....49
5.2.4 Additional H-Field and E-Field plots....51
5.2.5 Computed Power Dissipation Density....54
6 SAR Analysis....55
6.1 Centered Configuration....55
6.1.1 Computed SAR Results....55
6.2 Offset Configuration....58
6.3 FCC SAR Requirements....61
7 Summary....62
8 Statement of Compliance....63

Illustration Index

Illustration 1: Maestro Rechargeable System Components....3
Illustration 2: Detail photo of Rechargeable Neuroregulator and Leads....3
Illustration 3: Simplified block diagram of charging system....4
Illustration 4: Rendering of transmit coil assembly in XFdtd....6
Illustration 5: View of RNR device with coil as modeled in Remcom XFdtd....7
Illustration 6: Simulator rendering including tissue phantom....7
Illustration 7: Grid slice showing typical level of detail used in transmit coil PCB region. Cells are on the order of 0.2 mm on a side....10
Illustration 8: 3D CAD rendering of detail required in RNR coil mesh. Some materials were hidden to enable viewing of coil details....11
Illustration 9: TC and RNR Centered Orientation....15
Illustration 10: TC and RNR Offset Orientation....15
Illustration 11: B-Field Probe near TC Plane....16
Illustration 12: B-Field Probe between RNR and TC....16
Illustration 13: Oscilloscope images for centered configuration RNR measurements with B-Field probe between TC and RNR. See column 3 of Table 6....19
Illustration 14: Oscilloscope images for centered configuration RNR measurements and B-Field centered on TC. See column 2 of Table 6....20
Illustration 15: Oscilloscope images for centered configuration TC measurement with B-Field probe between TC and RNR. See column 3 of Table 7....21
Illustration 16: Oscilloscope images for centered configuration TC measurements and B-Field centered on TC. See column 2 of Table 7....22
Illustration 17: Oscilloscope images for offset configuration RNR tests with B-field probe centered between TC and RNR. See column 3 of Table 8....25
Illustration 18: Oscilloscope images for offset configuration RNR tests with B-field probe centered on TC. See column 2 of Table 8....26
Illustration 19: Oscilloscope images for offset configuration TC tests with B-field probe between RNR and TC. See column 3 of Table 9....27

Illustration 20: Oscilloscope images for offset configuration TC tests with B-field probe centered on TC. See column 2 of Table 9....28
Illustration 21: LT-Spice schematic diagram....29
Illustration 22: LTSpice computed waveforms for centered configuration....31
Illustration 23: LT-Spice schematic diagram....32
Illustration 24: LTSpice computed waveforms for offset configuration....34
Illustration 25: Top view of centered configuration....37
Illustration 26: Side view of centered configuration....37
Illustration 27: Computed current in TC and RNR coil....39
Illustration 28: Computed voltage at terminals of TC and RNR coil....39
Illustration 29: Centered configuration B-field slice in plane of TC....41
Illustration 30: Centered configuration B-field midway between TC and RNR....41
Illustration 31: Vertical slice computed H-Field at 0 degrees phase. Normalized to 1,000 A/m.. 43
Illustration 32: Vertical slice computed H-Field at 100 degrees phase. Normalized to 1,000 A/m. 43
Illustration 33: Vertical slice computed E-field at 0 degrees phase. Normalized to 10,000 V/m..44
Illustration 34: Vertical slice computed E-field at 100 degrees phase. Normalized to 10,000 V/m. 44
Illustration 35: Computed dissipated power density (W/m^3) vertical slice near center of simulation space....45
Illustration 36: Top view of offset configuration....46
Illustration 37: Computed current waveform in TC and RNR coil....48
Illustration 38: Computed voltages on TC and RNR....48
Illustration 39: Offset configuration B-field slice in plane of TC....50
Illustration 40: Offset configuration B-field slice midway between TC and RNR....50
Illustration 41: Computed H-Field at 0 degrees phase. Vertical slice. Normalized to 1,000 A/m. 52
Illustration 42: Computed H-Field at 100 degrees phase. Vertical slice. Normalized to 1,000 A/m....52
Illustration 43: Computed E-field at 0 degrees phase. Vertical slice. Normalized to 10,000 V/m. 53
Illustration 44: Computed E-field 100 degrees phase. Vertical slice. Normalized to 10,000 V/m. 53
Illustration 45: Computed dissipated power density (W/m^3) vertical slice near center of simulation space....54
Illustration 46: Vertical slice containing maximum 1 gr SAR....56
Illustration 47: Horizontal slice containing maximum 1 gr SAR....56
Illustration 48: Vertical slice containing maximum 10 gr SAR....57
Illustration 49: Horizontal slice containing maximum 10 gr SAR....57
Illustration 50: Vertical slice containing maximum 1 gr SAR....59
Illustration 51: Computed 1 gram SAR average in horizontal max slice 1.56 mm below TC.....59
Illustration 52: Vertical slice containing maximum 10 gr SAR....60
Illustration 53: Horizontal slice containing maximum 10 gr SAR....60

Index of Tables

Table 1: Revision History....v
Table 2: Maestro Rechargeable System Components and Model Numbers....2
Table 3: Material Properties used in FDTD simulation....9
Table 4: Calibration of the LEM Probe using Instek SFG-2110 Function Generator....12
Table 5: Beehive Electronics B-field Probe Data....13
Table 6: Centered Configuration results for RNR current and voltage measurement....17
Table 7: Centered Configuration results for TC current and voltage measurement....17
Table 8: Offset configuration results for RNR measurement....23
Table 9: Offset Configuration results for TC measurement....23
Table 10: Centered configuration timing information....30
Table 11: RMS and Peak values of circuit model parameters....30
Table 12: Offset configuration timing information....33
Table 13: RMS and Peak values of circuit model parameters....33
Table 14: Measured versus computed B-field for centered configuration....40
Table 15: Measured versus computed B-field for offset configuration....49
Table 16: General Population/Uncontrolled Exposure Limits (W/kg)....61
Table 17: Maximum computed SAR values....63

Table 1: Revision History

Report No.	Version	Description	Issued Date
ENT-FCC-2014-01	Rev. 01	Initial issue of report	Dec 5, 2014
ENT-FCC-2015-01	Rev. 02	Address FCC response of December 30, 2014	Mar 5, 2015
ENT-FCC-2015-02	Rev. 03	Address FCC response of March 17, 2015	Mar 17, 2015
ENT-FCC-2015-03	Rev. 04	Address FCC response of March 27	Mar 29, 2015

1 Purpose

The purpose of this report is to document the Specific Absorption Rate (SAR) analysis of the EnteroMedics Maestro® Rechargeable System (also known as the Maestro® RC System) for the Federal Communications Commission (FCC).

The work described herein was carried out by Mr. John Ross with assistance from Mr. Scott Lambert, Mr. Koen Weijand, Mr. Mark Bosshard, and Ms. Wendy Barron. Mr. Ross is a consulting engineer specializing in antennas and applied electromagnetics. He has a Ph.D. in Electrical Engineering from Michigan State University and is a licensed Professional Engineer in the state of Utah. Mr. Lambert is employed by EnteroMedics as the Director of Engineering. He has a Bachelor of Science in Electrical Engineering from the University of Minnesota. Mr. Weijand is the principle designer of the systems documented here and a consultant to EnteroMedics Inc. He has a Master of Science in Electronic Engineering from Delft University, The Netherlands. Mr. Bosshard is a SolidWorks CAD designer contracted by EnteroMedics. He has a Bachelor of Science in Industrial Education from Winona State University. Ms. Barron is an electronic technician. She has an Associate in Applied Science in Electronic Technology from Anoka Technical College and a Bachelor of Arts in Biology from Metropolitan State University.

1.1 Revisions

This report is a substantial update of report ENT-FCC-2014-01. It addresses issues raised by the FCC in a December 31, 2014 communique and includes updated results for two different configurations of the EnteroMedics device. The SAR simulations are based on measurements taken when the RNR is being charged by the mobile charger and transmit coil, which is the maximum power transfer condition. The first configuration is the nominal or centered configuration which represents the device in typical operation. The second configuration is a worst case or offset configuration which produces maximum RF power in laboratory measurements. This configuration is not typically encountered in normal operation but is included to assess worst case operating conditions. These two configurations represent the range of coupling of the system to ensure that the nominal to worst case conditions are included in the SAR computational modeling. The field values produced by the simulator were seen to correlate well with laboratory measurements of magnetic fields near the device. The 1 gram and 10 gram SAR averages were again shown to be in compliance with the limits set forth by the FCC.

1.2 Scope

The SAR analysis described in this report applies only to the following product:

Manufacturer: EnteroMedics Inc.

Models: 200 Maestro Rechargeable System

2002 Rechargeable Neuroregulator

2402 Mobile Charger

2403-60 Transmit Coil

FCC ID: 2ABHRMC2402

The computational modeling results in this report apply exclusively to the simulated model / samples listed above.

1.3 System Overview

The Maestro Rechargeable System is a Class III medical device intended for the treatment of obesity and obesity related disorders.

The Rechargeable Neuroregulator (RNR) and leads are the implantable parts of the system. The RNR and leads are used to deliver electrical current to the vagal nerve. The RNR has an integrated coil antenna cast around the perimeter of the device. The RNR connector ports are 3.2 mm IS-1 compatible to allow connection with the 3.2 mm IS-1 compatible connectors on the leads. Two leads are implanted; one for the anterior and one for the posterior vagal nerve trunks.

The Mobile Charger (MC) is an external device that is used to communicate with the RNR and to charge the RNR through the detachable Transmit Coil (TC) antenna.

The Clinician Programmer (CP) is used to program therapies and read device logs. The CP connects to the MC through the Programmer Cable.

The AC Recharger is used to charge the MC battery by directly connecting the AC Recharger to the same port that is used to connect the MC to the transmit coil.

A list of the system subcomponents that may be used for testing are shown in Table 2. Photographs of the various system components are shown in Illustration 1. A close up view of the rechargeable neuroregulator and leads is shown in Illustration 2.

Component	Model Number
Implantable Components	
Rechargeable Neuroregulator (RNR)	2002
Posterior Lead	2200P-47E
Anterior Lead	2200A-47E
External Components	
Mobile Charger (MC)	2402
Transmit Coil (TC)	2403-60
AC Recharger	1620
Clinician Programmer (CP)	2502
Programmer Cable	1600

Table 2: Maestro Rechargeable System Components and Model Numbers

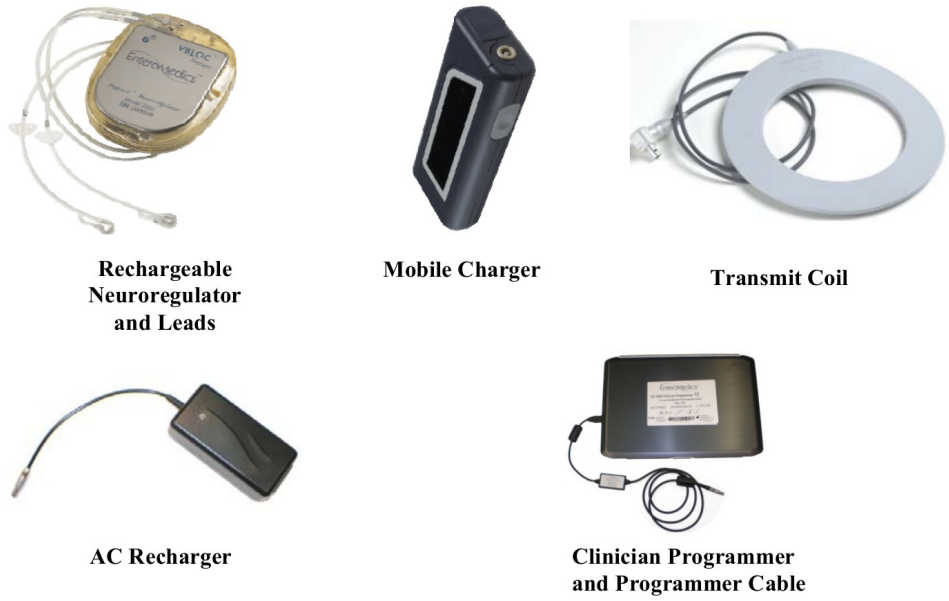

Illustration 1: Maestro Rechargeable System Components

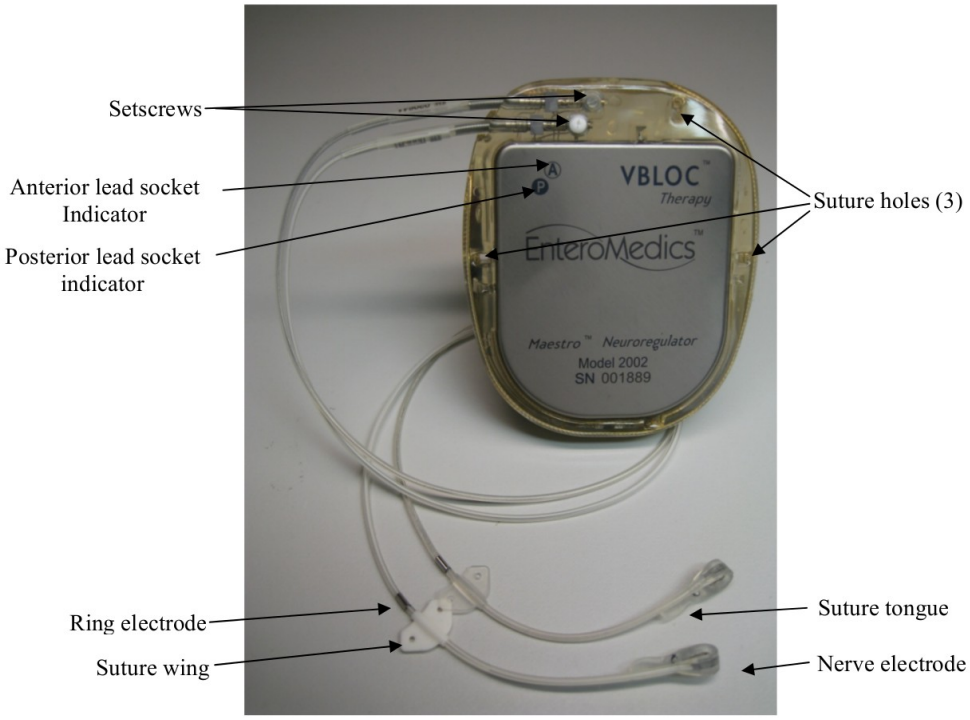

Illustration 2: Detail photo of Rechargeable Neuroregulator and Leads

1.4 System Operation

This section describes the inner workings of the system in order to provide a basis for the approach used to efficiently compute the SAR exposure during RF charging of the RNR battery.

1.4.1 Charging Procedure

The patient finds the optimum antenna position when placing the antenna over the implant site, guided with help of indicators on the mobile charger. The patient then initiates charging. The mobile charger periodically interrupts charging to communicate RNR battery status and charging parameters and then automatically resumes charging until the RNR is fully charged or the mobile charger battery is depleted.

1.4.2 Inductive System Description

The frequency of energy transmission between the TC and the RNR coil is at an ISM band frequency of 6.78MHz. The mobile charger generates a B-field using a high Q resonating antenna coil. The RNR antenna coil, also high Q, is tuned at 6.78MHz and converts the received B-field effectively into a current to charge the battery.

A simplified block diagram of the charging system is shown in Illustration 3. The two resonating tanks of mobile charger transmitter and RNR receiver form a set coupled coils and the impedance of the set of coils varies with the separation distance. A control mechanism in the transmitter is designed to regulate the power to the transmit antenna to minimize the effect of variation of separation or coupling. This control mechanism has a response time in the order of a few of milliseconds.

The set of coupled coils form a bandpass filter with a step response that is dependent on the coupling distance. For the recommended 2.5cm implant depth it takes approximately 5 micro-seconds (µs) or 34 cycles of the 6.78 MHz wave until the system is in steady state. The amplitude regulation mechanism that compensates the variation of distance, is slower and adds more time before the system is in a steady state. A total of 100 cycles of 6.78 MHz are expected to be needed before the amplitudes have stabilized. As will be shown in subsequent sections, this long settling time leads to problems in the calculation of the SAR using time domain based electromagnetic field simulators.

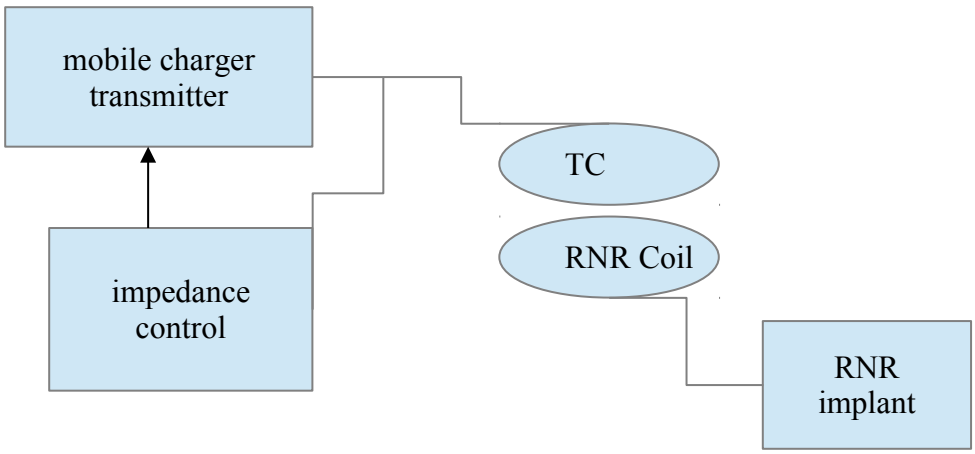

Illustration 3: Simplified block diagram of charging system.

2 SAR Analysis Overview

This section reviews the tools used in the SAR analysis and some of the assumptions and approximations used in the calculations.

2.1 Software and Computer Tools

The SAR analysis documented here is carried out using the Remcom XFdtd software version 7.4.0.5 released in late 2014. Remcom (www.remcom.com) is a maker and seller of electromagnetic simulation software based in State College, PA. Remcom tools are considered to be state-of-the-art in the high frequency EM simulator industry.

The Remcom XFdtd software uses an accepted algorithm known as FDTD (Finite Difference Time Domain) to compute the electromagnetic fields. SAR is subsequently computed using FCC compliant algorithms for 1 gram and 10 gram averages. The simulation code validation has been conducted pursuant to IEC 62704-4 DRAFT with results submitted as a separate Operational Description exhibit.

For this analysis, the Remcom XFdtd software was run on a custom GPU (Graphics Processing Unit) workstation running the Xubuntu 14.04.1 operating system. Xubuntu is a member of the widely used Ubuntu family of Linux operating systems produced by Canonical Corporation of South Africa. The custom workstation has an 8-core AMD CPU (Central Processing Unit) running at 4.0 GHz, 32 GB of ECC (Error Correcting Code) RAM and a 250 GB SSD SATA-III (Solid State Disk). It also has four nVidia Fermi class (e.g. Tesla C2070 and Quadro 6000) GPUs that can be used to dramatically accelerate the FDTD calculations. Each Fermi GPU has 448 GPU cores and 6 GB of ECC video RAM. In total, the GPU workstation has 1792 GPU cores and 24 GB of video RAM and is capable of producing over 4 TeraFLOPS of single precision throughput.

Despite the considerable power of the Remcom software and the associated GPU workstation, numerous approximations must be made in the configuration of a simulation if useful results are to be produced in a reasonable amount of time.

2.2 CAD Modeling

Fundamental to the modeling of the device is obtaining an accurate CAD model of the critical components of the system. Relevant solid model CAD files were provided by Mr. Bosshard. Relevant PCB CAD files were provided by Mr. Lambert.

A CAD rendering of the transmit coil assembly in the Remcom XFdtd is shown in Illustration 4. Transparency is enabled so that details internal to the silicone over mold can be seen. Solid model components were exported from original SolidWorks CAD files in the industry standard STEP format. PCB (Printed Circuit Board) traces were exported from the original PCB CAD tools in industry standard ODB++ format. The various CAD files were imported into the Remcom XFdtd simulator and combined to arrive at an accurate model suitable for the purpose of computing SAR.

The cable that leads from the Transmit Coil (TC) to the Mobile Charger (MC) was omitted from the model since it is a shielded cable that provides a negligible contribution to the SAR. A view of the RNR device model with transparency is shown in Illustration 5. The interior circuit elements of the RNR device are extremely complicated and impossible to model using the Remcom simulator or any other known and commercially available full wave electromagnetic simulator. To get around this difficulty, the interior of the titanium shell is modeled as being air filled and the RNR coil is terminated in a simple

Norton equivalent current source. This model is valid since the hermetically sealed titanium shell acts as a Faraday cage preventing electromagnetic energy from the outside from appearing on the inside and visa-versa except via the coil terminals. The motivation for, and details of the Norton equivalent current source termination are described later.

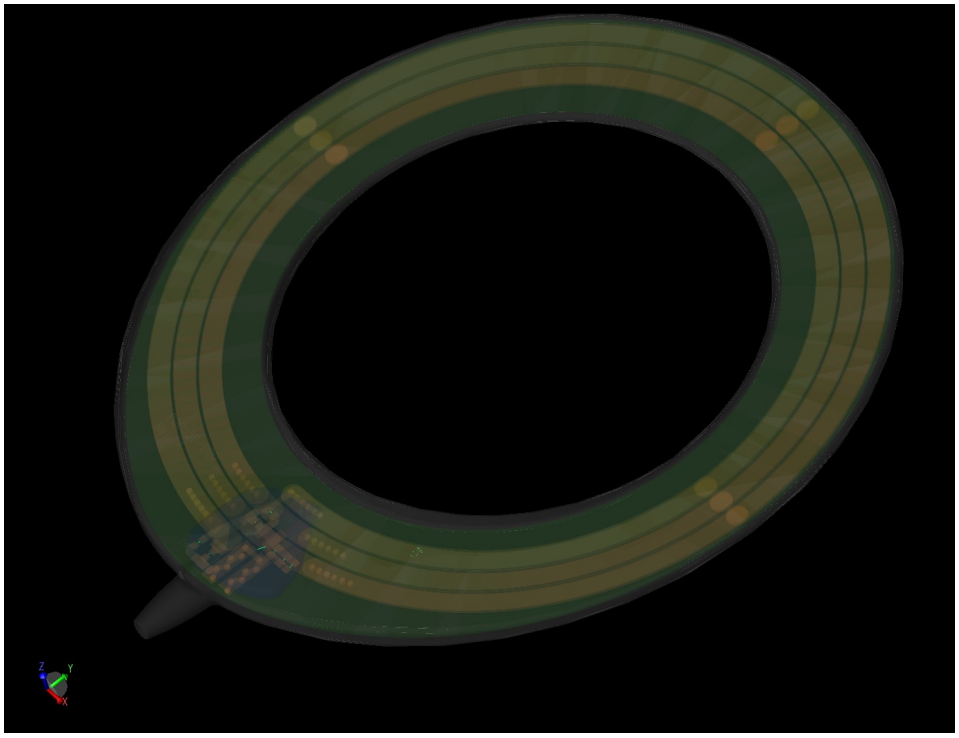

Illustration 4: Rendering of transmit coil assembly in XFdtd.

Omission of the leads is justified since they are common mode filtered with an equivalent series impedance of 2000 ohms at the operating frequency of 6.78 MHz internally to the RNR device. A test was performed to demonstrate that the leads have an insignificant effect on SAR. An RNR was charged with the leads positioned to achieve the highest coupling to the transmit coil by routing the leads in separate directions in a circle around the RNR while submerged in saline with a physiologic impedance of 1000 ohms. This lead routing is not a configuration that is possible to be used for an implant but represents a worst case test configuration. The leads develop 3000 times less current (205 uA RMS) than is developed in the RNR coil. As a result, the leads would have an insignificant effect on SAR when compared to the SAR produced by the transmit coil and RNR coil.

A CAD rendering of a complete model along with a rectangular slab of homogeneous tissue phantom (red) is shown in Illustration 6. The dimensions of the tissue phantom and the position and orientation of the transmit coil and RNR device can easily be adjusted to suit different operational conditions. In normal operation, the transmit coil is flush to the skin with a thin layer of clothing in between. The SAR model neglects the clothing layer and places the transmit coil directly on the tissue phantom boundary. This is a worst case scenario for the transmit coil placement. The region of the solution space includes the tissue phantom as well as a region of free space (air) above the transmit coil. This solution space is terminated on all sides using a 7-layer PML (Perfectly Matched Layer) boundary condition. This boundary condition minimizes boundary reflections and ensures accuracy of the field and SAR calculations inside the solution space.

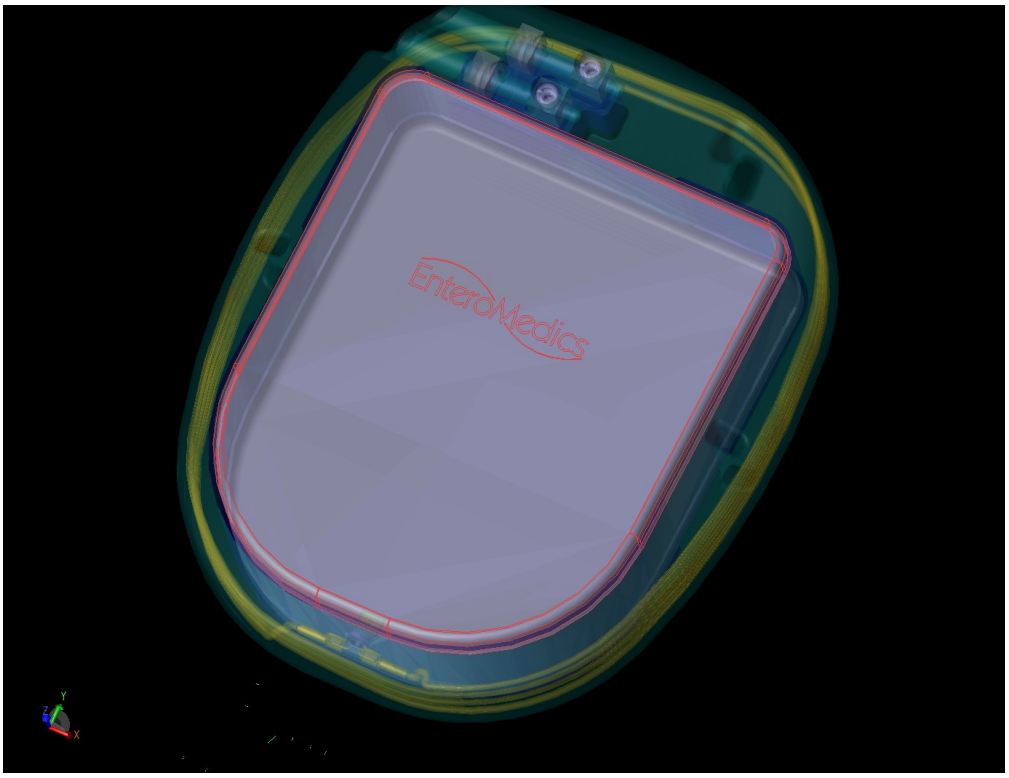

Illustration 5: View of RNR device with coil as modeled in Remcom XFdtd

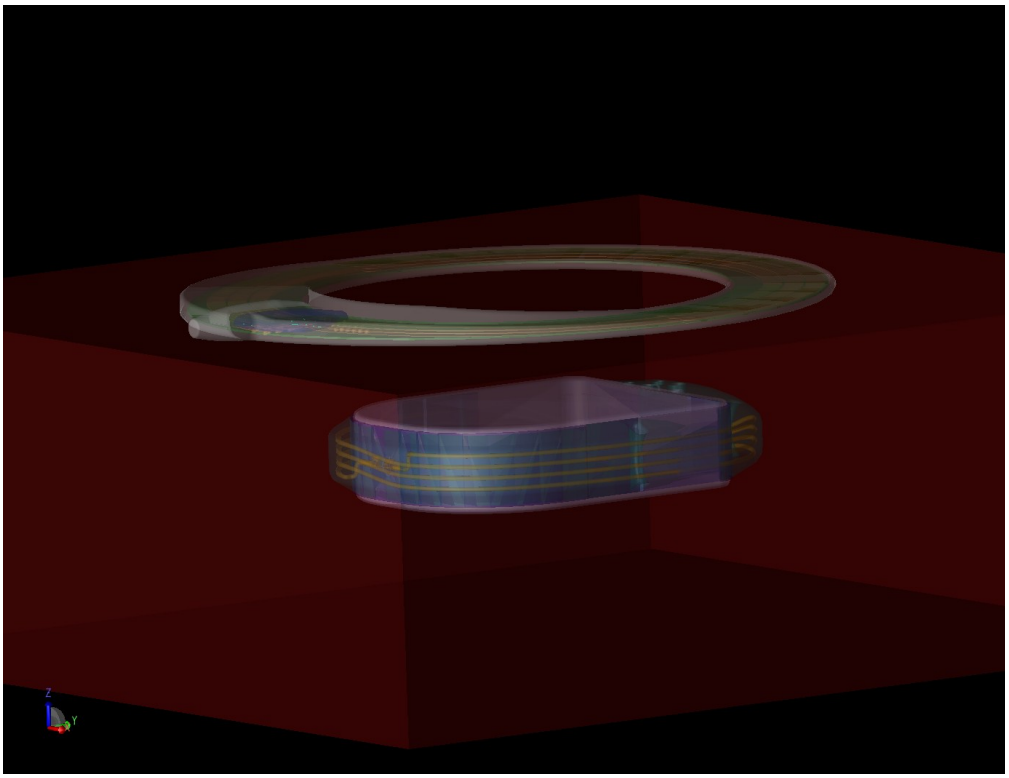

Illustration 6: Simulator rendering including tissue phantom

2.3 Material Properties and Tissue Modeling

Accurate characterization of material properties is critical to the accuracy of FDTD simulations. The Remcom simulator includes a limited library of electrical material properties for various metals, general dielectric materials, and materials produced by manufacturers for use as electronic substrates. The conductivity figures for the metals (e.g. Copper, Gold, Titanium, etc.) used in the EnteroMedics devices were either in the Remcom library or relatively easy to find in the literature.

Obtaining information on dielectric materials is significantly more difficult. At this time, some of the materials used in the EnteroMedics model do not have accurate characterization of dielectric constant and conductivity / loss tangent at the operating frequency of the device. This is not an unusual situation in the electronics industry. Indeed, laboratory characterization of every material used in a modern device is not usually feasible due to the overwhelming cost and time required to generate such data at all of the appropriate frequencies. While dielectric constant and conductivity data is available for some materials, the data is almost universally limited to frequencies in the kHz and low MHz range. Dielectric properties at higher RF frequencies are often difficult or impossible to find in the literature.

EnteroMedics has provided material data sheets for the epoxy and silicone used in the TC assembly, but the manufacturer only provides electrical data a single frequency (~1 kHz) which is considerably lower than the operating frequency (~ 6.78 MHz). Nonetheless, this is the best available data at this time.

To date, no official data has been located for the Tecothane material used to surround the RNR coil assembly. The Lubrizol website (https://www.lubrizol.com/LifeScience/Products/Tecothane.html) indicates that "Techothane™ aromatic polyether-based thermoplastic polyurethanes (TPUs) are unique resins which exhibit solvent resistance and biostability over a wide range of hardnesses." Polyurethane type materials are generally known to have dielectric constants on the order of about 6.3 and loss tangents of about 0.002 at RF frequencies (http://globalpolymer.com/documents/uhmw_specs.pdf). This is generic data however and actual parameters may vary from this assumed value. This is the best available data for Tecothane at this time.

The most critical material in this simulation however is the one used for the tissue or body phantom. In e-mail communications on July 30, 2014 with the TUV TCB on behalf of EnteroMedics concerning the device, the FCC has indicated:

> ***"For modeling devices with frequencies approaching 10 MHz, a relative permittivity of 211 and a conductivity of 0.63 would be acceptable for a homogeneous model."***

A later e-mail communication from the FCC on October 10, 2014 with the TUV TCB on behalf of EnteroMedics indicated that:

> ***"Dielectric constant of 211 and conductivity of 0.63 S/m represent the average values for the two types of muscle fiber calculated by the 4-Cole-Cole equation in the 1996 Air Force report which is referenced on the FCC website. Average muscle represents a conservative setup for generic exposure conditions with homogeneous tissue blocks. http://transition.fcc.gov/oet/rfsafety/dielectric.html"***

Based on these remarks, the tissue phantom was modeled as a homogeneous slab with relative permittivity of 211 and conductivity 0.63 S/m at the operating frequency of 6.78 MHz. A tissue density of 1000 kg / m^3 was used. The dimensions of the homogeneous tissue slab were adjusted to minimize computational resources while avoiding boundary reflection issues.

The rectangular body phantom slab has dimensions 180 mm x 180 mm x 75 mm and contains the RNR. An air region of dimensions 180 mm x 180 mm x 20 mm is present above the body phantom and contains the transmit coil.

Details of the locations of the various components relative to the body phantom boundaries is is provided for each configuration in subsequent sections.

A list of all material types and tissues used in the model, their use, and their associated electrical material properties are provided in Table 3.

Material Type	**Usage**	**Relative Permittivity**	**Loss Tangent**	**Conductivity (S/m)**
Air	Fill region above transmit coil	1	0	
Alumina – 96%-99%	Insulator for RNR coil to case pass thru	9.8	0.0002	
Copper	Transmit coil PCB traces	1		5.98×10^{7}
EPO-TEK H67-MP	Epoxy for transmit coil and RNR shell	4.9	0.0041	
FR4 Glass Epoxy	Transmit coil PCB Substrate	4.35	0.017	
Gold	Coating on RNR coil wire	1		4.26×10^{7}
MP35N alloy	Lead connections	1		984252
Muscle fiber	Body phantom per FCC	211		0.63
Polytetrafluroethylene	RNR coil wire jacket	2.0	0.0002	
Silicone	Cover material for transmit coil	2.86	0.006	
Solder	Component connections as needed	1		6.67×10^{6}
Stainless Steel (316L)	Lead connection	1		1.351×10^{6}
Tecothane TT-1075 D-M	Surround material for RNR coil	6.3	0.002	
Titanium	RNR case and lead connections	1		2.33×10^{6}

Table 3: Material Properties used in FDTD simulation.

2.4 Cell Size versus Memory and Run-time Requirements

In the FDTD method, the Yee cell must be sized such that it is less than approximately 1/15 of an electrical wavelength on a side. The electrical wavelength in this case is to be computed in the material being modeled.

The wavelength of a 6.78 MHz electromagnetic wave in free space is approximately 44.22 meters. The highest dielectric constant in the simulation is the tissue phantom. In this medium, the wavelength is still on the order of approximately 3 meters and the maximum Yee cell size is approximately 0.2 meters. In the case of the EnteroMedics device, the cell size is dictated by the need to capture relevant geometrical detail instead of meeting requirements based on electrical wavelength.

An example of the level of detail required to model the EnteroMedics transmit coil is shown in Illustration 7. Here a grid cross section near the feed point region of the transmit coil is modeled using cells of approximately 0.2 mm on a side. The Remcom XACT conformal cell technology is enabled to

retain sub-cellular size detail for conducting elements. A similar level of detail is required to model the RNR coil as shown in 3D mesh rendering of Illustration 8. The close spacing of the traces on the transmit coil and on the RNR coil and the meshing strategies of the Remcom code ensure that cell sizes are on the order of 0.2 mm throughout most of the solution space. This fine level of detail combined with the long stabilization time of the Neuroregulator charging system proved to be somewhat problematic for the FDTD algorithm used in the Remcom simulator.

The small cell size required to capture essential geometry detail in the TC and RNR coil regions resulted in a mesh of approximately 65 million Yee cells. It also lead to a very small time step (~ 1.29×10^{-7} µs) in order to meet the Courant condition and ensure stability of the FDTD algorithm. The net effect was that more than 1 million time steps were required to compute the response over a single oscillation of the 6.78 MHz sine wave. With the large mesh size, the calculation for a single oscillation required over 10 hours using all 1800 cores on the GPU workstation. It was therefore impractical to compute the 30 to 100 or more oscillations that would be required to allow a transient solution to naturally come to steady state in the FDTD simulator.

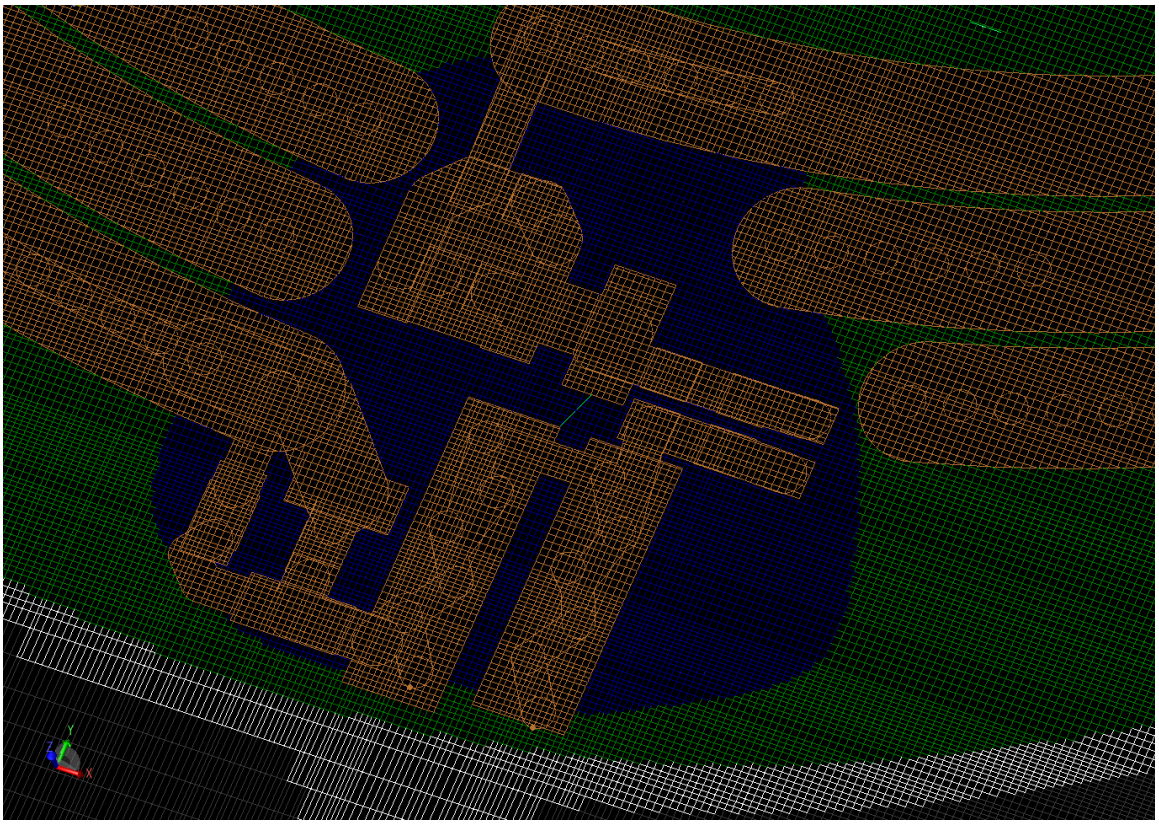

Illustration 7: Grid slice showing typical level of detail used in transmit coil PCB region. Cells are on the order of 0.2 mm on a side.

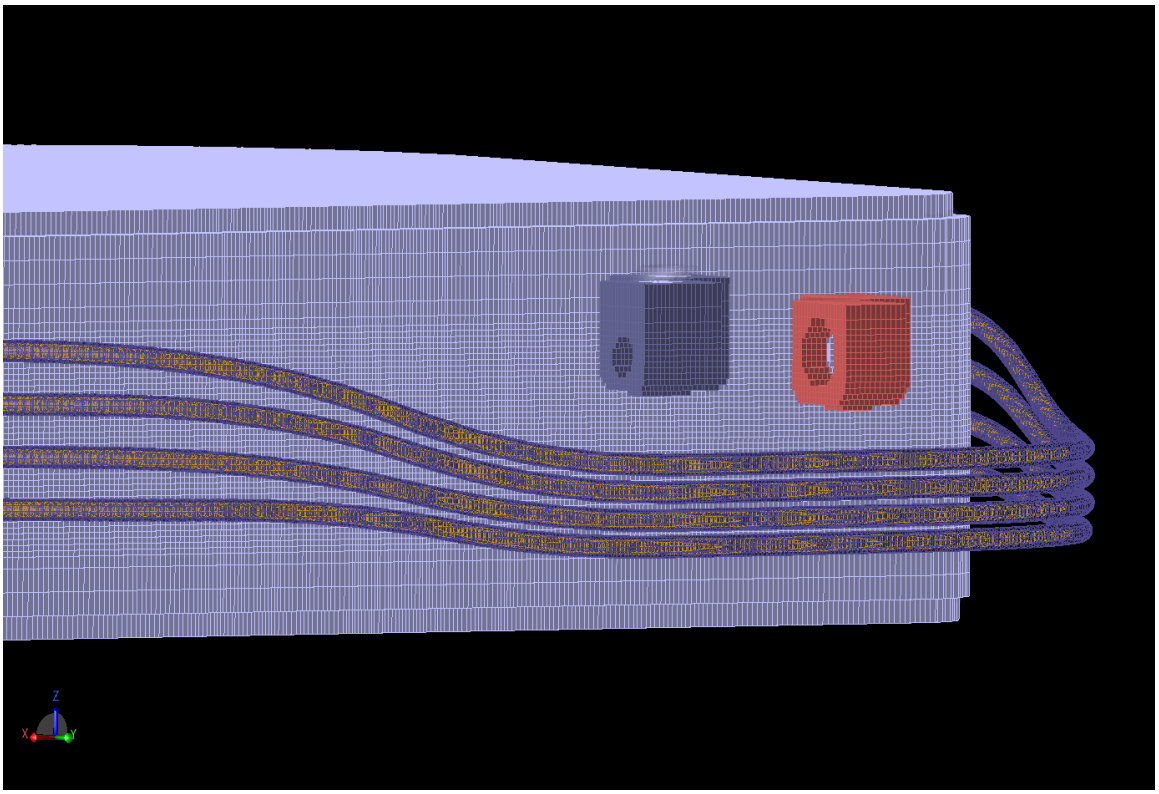

Illustration 8: 3D CAD rendering of detail required in RNR coil mesh. Some materials were hidden to enable viewing of coil details.

2.5 Source Modeling Approach

To reduce simulation run-times to a manageable level, a novel means of jump starting the FDTD simulation to a sinusoidal steady state condition was devised. The method used measured current and voltage data from the actual device. Sinusoidal currents based on these measurements were then injected into the coils in the Remcom simulator by means of ideal Norton equivalent current sources. This approach eliminated the need to use any resonant circuits and greatly reduced required run times. Run times were still significant however.

Attempting to directly measure the actual voltage and current on the coils results in a detuning of the tank circuit. Therefore, secondary voltages and currents were measured using a current probe. The actual antenna coil voltages and currents were subsequently derived from the measurements using Spice circuit simulations.

The laboratory measurements used to determine the source model as well as the near-zone magnetic flux density (B-field) measurements used to validate the simulation are described in the next section.

3 Laboratory Measurements

This section is essentially an edited and reformatted version of an internal test report produced by Ms. Barron to suit the purposes of this FCC SAR report. The work was carried out between January 26 and January 29, 2015.

3.1 Purpose

The purpose of this work was to obtain voltage, current and phase measurements necessary to provide inputs for the SAR computational models and to measure B-field for verification of the SAR computational models. The measurements are taken when the RNR is being charged by the mobile charger and transmit coil, which is the maximum power transfer condition.

3.2 Equipment Used

- MC SN D05120 FW version 5.04
- RNR Development Circuit Assembly P00371-000 SN 4 FW version 2.21 with RNR Header/Coil Assembly SN 10; Center Frequency = 6.910MHz Q=28.84
- Transmit Coil SN SAR Test; Center Frequency = 6.774MHz, Q=312
- Tektronix TPS 2024B Oscilloscope ID 808 Calibration due 30 Nov 2015
- Instek SFG-2110 Function Generator ID E90222 Calibration due 31 Dec 2015
- LEM Probe LS50 Calibration - See calibration data in Table 4 below:

Voltage P-P	Voltage RMS	Measured Current P-P	Measured Current RMS	Expected Current P-P	Expected Current RMS
20V	6.9V	0.40A	0.133A	0.40A	0.138A
10V	3.3V	0.21A	0.068A	0.20A	0.066A

Table 4: Calibration of the LEM Probe using Instek SFG-2110 Function Generator

- B-Field Probe Beehive Model 100A SN 1018 Calibration due 31 Dec 2016

3.3 B-Field Probe Conversion Formula

According to Beehive Electronics, the formula to convert B-field probe measurements to B-field values is given by:

$$B = 10^{\left(\frac{(Pout - X - 20\log_{10}(F))}{20}\right)} \quad (1)$$

where

B is the magnetic flux density in Tesla (T),
F is the frequency in MHz,
Pout is the probe output power into 50 ohms expressed in dBm,
and X is a probe dependent scale factor given in Table 5.

Model Number	X	3 dB Frequency (MHz)	First Resonance (MHz)
100A (medium loop)	65.2	1000	2600

Table 5: Beehive Electronics B-field Probe Data

As required above, the formula for converting voltage to power in dBm with a 50 ohm scope load is given by:

$$Pout = 10\log_{(10)}\frac{V^2}{50} + 30 \qquad dBm \quad (2)$$

It is noted that the above relationship yields peak power when using peak values of voltage and average power when using RMS voltage values.

3.4 Test Configurations

Development versions of the Rechargeable Neuroregulator (RNR) and transmit coil were used to allow direct measurements of the voltage and current. A mechanical test fixture was used to reliably and repeatably hold the various components in the prescribed configurations. The fixture is made of acrylic plastic and has an insignificant effect on device operation.

Per FCC requirements, the measurements were made under the highest power output condition of the Mobile Charger (MC) charging the RNR.

Measurements were made with the TC and RNR in two different arrangements as follows:

1. Centered - RNR centered on the TC as shown in Illustration 9. This configuration represents typical use.
2. Offset - RNR offset from the center of the transmit coil as shown in Illustration 10. This configuration represents worst case use and produced the highest B-fields at the center coil positions discussed later.

In both of the above arrangements, the recommended 2.5 cm implant depth spacing between the transmit coil and the top of the RNR was used.

It is noted that in each case, the orientation of the TC windings and RNR coil windings were counter clockwise when referenced from the top looking downward. This is the specified method of operation and it ensured by the clear definition of a top and bottom orientation for the TC when it is enclosed in it's silicone covering.

Voltage measurements were made across the coaxial cable connections at the junction of the coaxial cable and antenna on the transmit coil and across C47 (1.5 nF) on the RNR circuit assembly.

TC current measurements were made using the center conductor of the transmit coil with the LEM current probe arrow pointing toward the transmit coil antenna. RNR coil current measurements were made using the RNR coil wire exiting the bottom of the RNR header/coil assembly with the LEM probe arrow pointing toward the RNR circuit assembly.

3.5 B-Field Probe Locations

For each of the TC-RNR configurations, the Beehive Model 100A medium sized B-field probe was positioned in two locations as follows:

1. Centered and near the plane of TC – This configuration is shown in Illustration 11. The loop of the probe was oriented to be in the same plane as the TC. In this configuration it is sensitive to the vertical (z-component) of B-field.
2. Centered on the TC in a plane midway between the TC and the top of the RNR – This configuration is shown in Illustration 12. Again, the loop of the probe was oriented to be in a plane parallel to the plane of the TC so that it was sensitive to the vertical (z-component) of the B-field. The plane containing the loop is approximately 12.5 mm below the plane of the TC.

The voltage signal provided by the B-field probe was used as the trigger reference in the voltage and current measurements. Results showed that changes in the probe location did not cause significant changes in the measured currents and voltages.

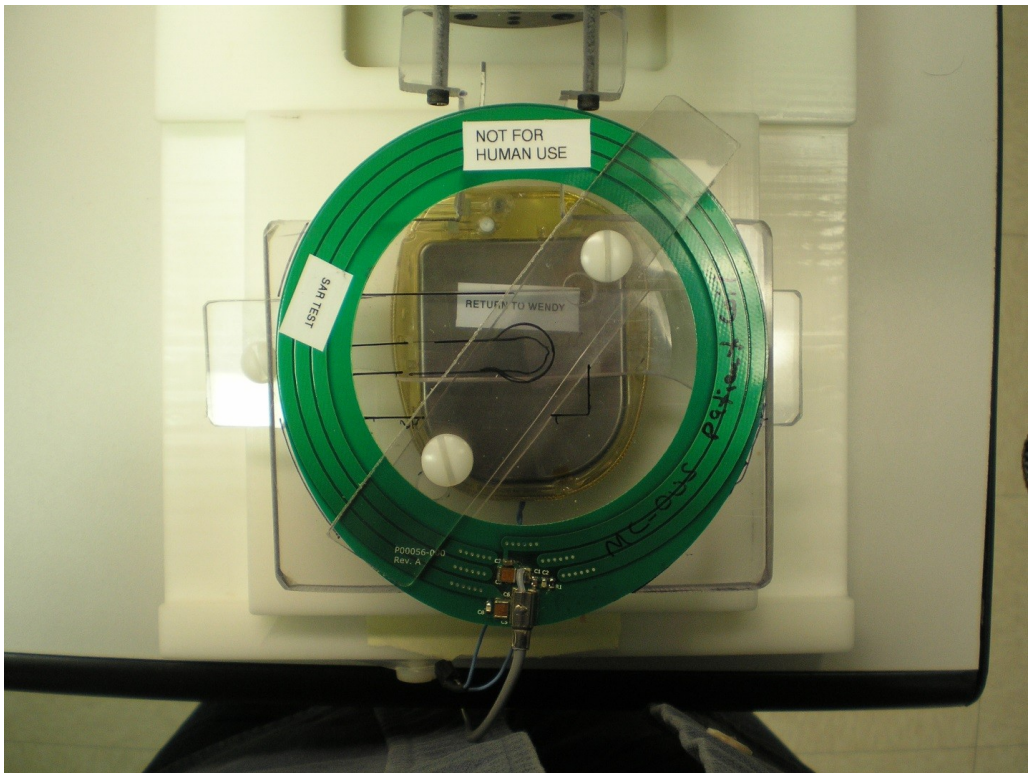

Illustration 9: TC and RNR Centered Orientation

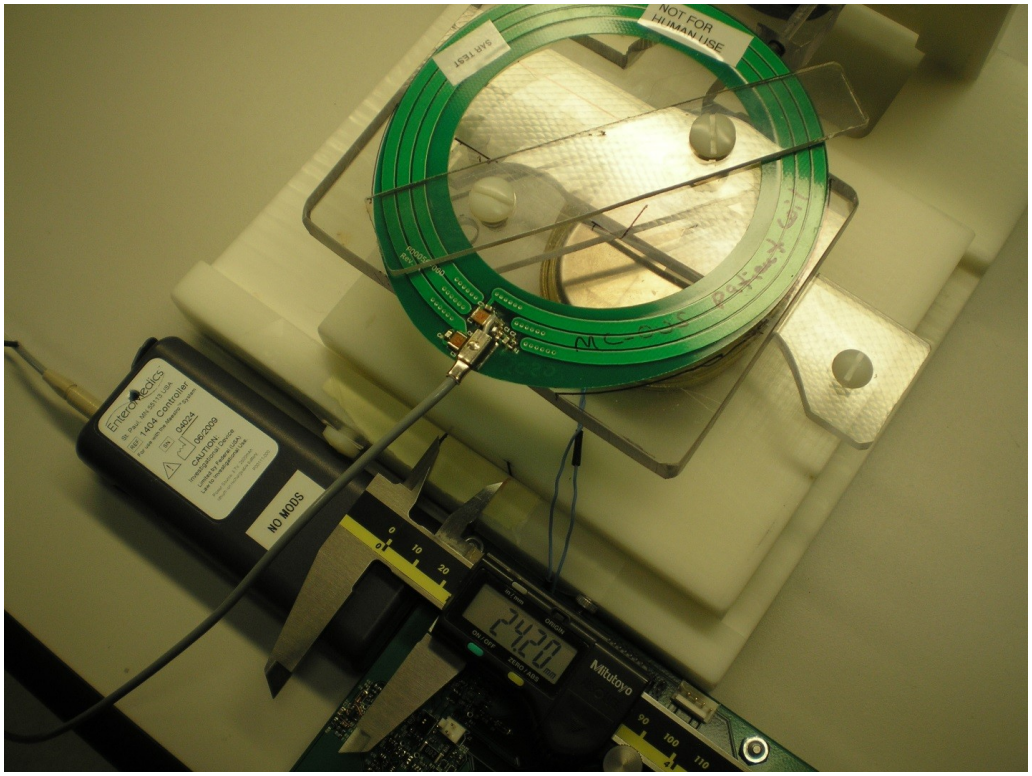

Illustration 10: TC and RNR Offset Orientation

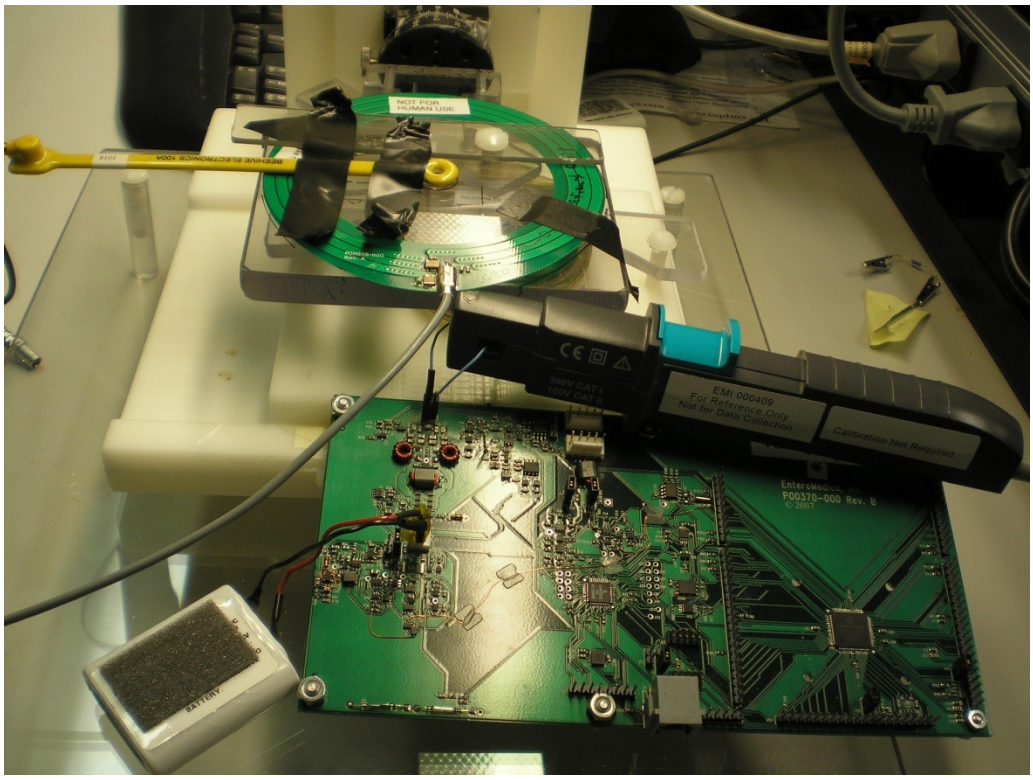

Illustration 11: B-Field Probe near TC Plane

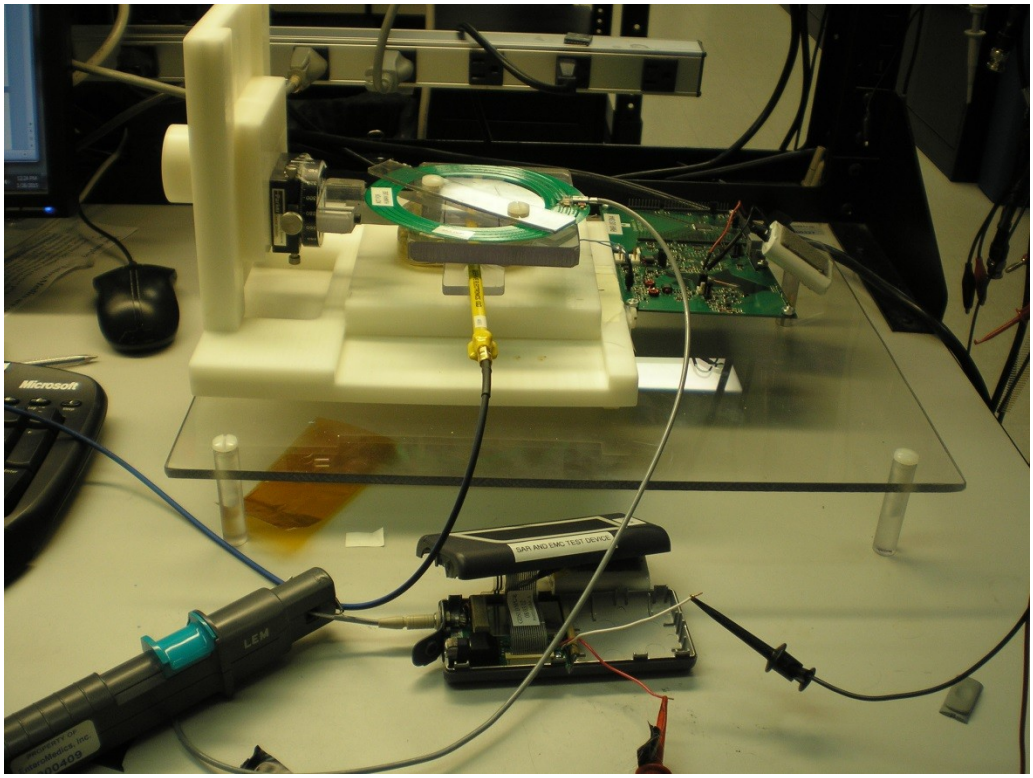

Illustration 12: B-Field Probe between RNR and TC

3.6 Centered Configuration Results

The summary results for the centered configuration current and voltage tests on the RNR are shown in Table 6. Corresponding oscilloscope images are shown in Illustration 13 and Illustration 14.

Test Parameter	B-Field Probe on Transmit Coil	B-Field probe between TC and RNR
RNR Voltage	4.55V	4.69V
RNR Current	613mA	633mA
B-Field Probe Voltage	52.5mV	30.5mV
B-Field during RNR measurement	19.0uT	11.1uT
Time delay for RNR Voltage compared to B-Field	30.4ns	25.2ns
Time delay for RNR Current compared to B-Field	14.8ns	10.4ns

Table 6: Centered Configuration results for RNR current and voltage measurement.

The summary results for the centered configuration current and voltage tests on the TC are shown in Table 7. Corresponding oscilloscope images are shown in Illustration 15 and Illustration 16.

Test Parameter	B-Field Probe on Transmit Coil	B-Field probe between TC and RNR
Transmit Coil Voltage	8.59V	8.63V
Transmit Coil Current	324mA	325mA
Transmit Coil Input Power	2.78W	2.80W
B-Field Probe Voltage	52.7mV	30.1mV
B-Field during TC measurement	19.1uT	10.9uT
Time delay for TC Voltage compared to B-Field	-67ns	-70ns
Time delay for TC Current compared to B-Field	-50ns	-55ns
RNR Battery Charge Current	224mA	223mA

Table 7: Centered Configuration results for TC current and voltage measurement.

Note that there is little difference between the B-field values when testing the RNR or TC provided the probe is fixed in the same location. Similarly, there is only a small change in measured voltage and current on either the RNR or TC with the probe in different locations. This consistency suggest that the probe does not significantly perturb the coupling between the TC and RNR.

There is a modest difference in the B-field measurements at the different probe locations. This is expected and consistent with simulation as is shown in the next section.

All measurements are in RMS except for RNR battery charge current. All channels are AC coupled. Channel 3 is terminated in 50 ohms to facilitate power measurement from the B-field probe.

As can be seen in Table 7 above, the mobile charger regulates the power level delivered to the transmit coil to approximately 3 W RMS in all cases.

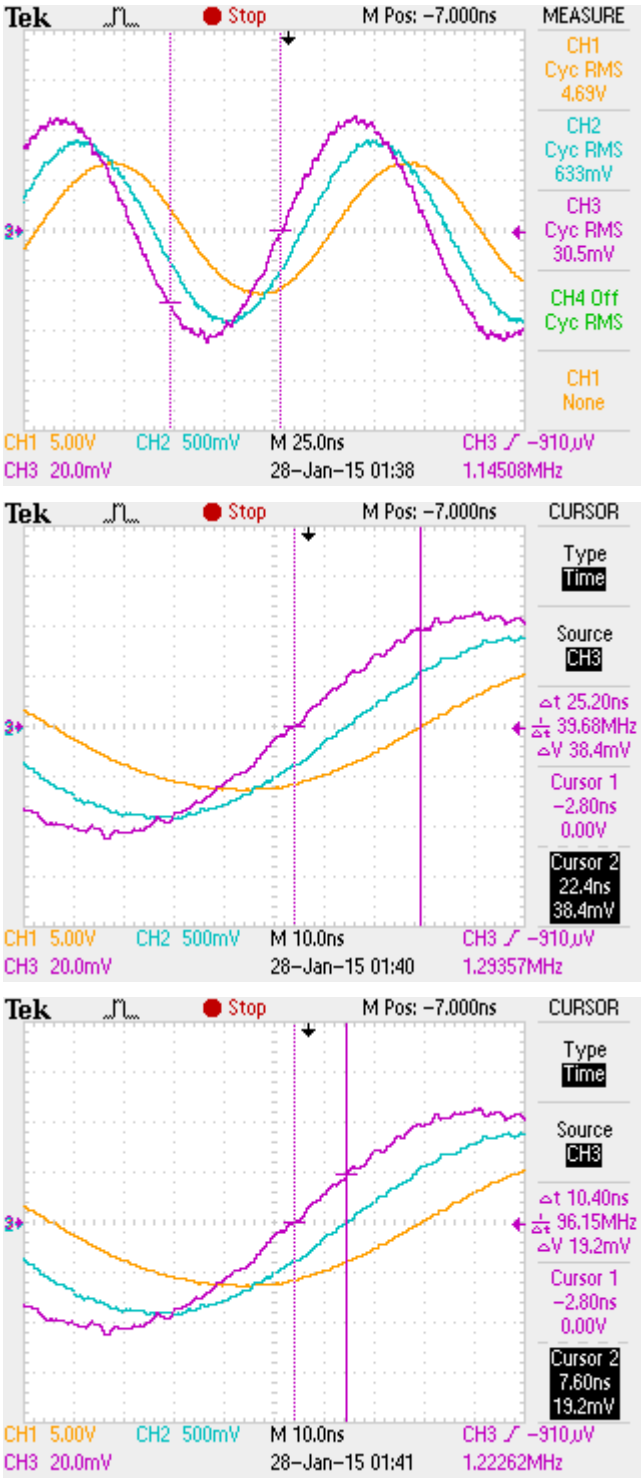

Channel 1 –Yellow = RNR tank voltage

Channel 2 – Blue = RNR current

Channel 3 – Purple = Model 100A B-Field probe voltage

Top Image - Voltage and Current Amplitudes

Middle Image - RNR tank voltage phase difference relative to the B-Field probe

Bottom Image - RNR current phase difference relative to the B-Field probe

Illustration 13: Oscilloscope images for centered configuration RNR measurements with B-Field probe between TC and RNR. See column 3 of Table 6.

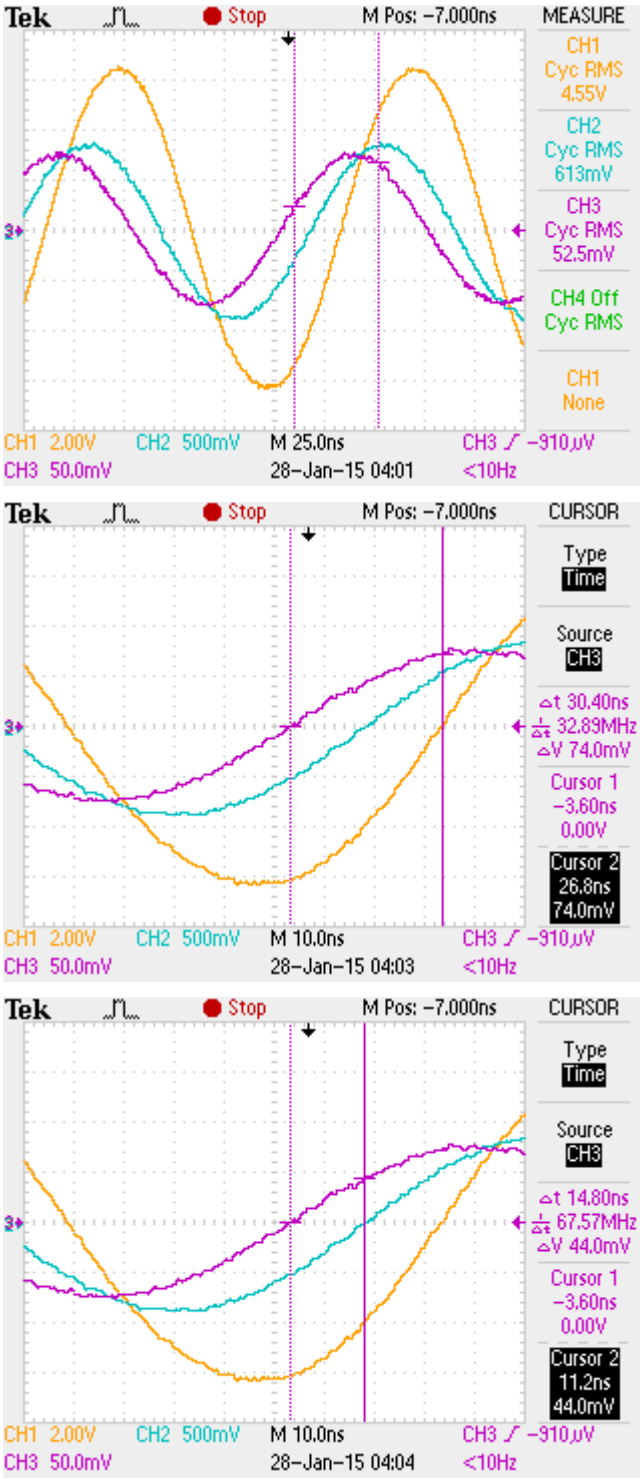

Channel 1 –Yellow = RNR tank voltage

Channel 2 – Blue = RNR current

Channel 3 – Purple = Model 100A B-Field probe voltage

Top Image - Voltage and Current Amplitudes

Middle Image - RNR tank voltage phase difference relative to the B-Field probe

Bottom Image - RNR current phase difference relative to the B-Field probe

Illustration 14: Oscilloscope images for centered configuration RNR measurements and B-Field centered on TC. See column 2 of Table 6.

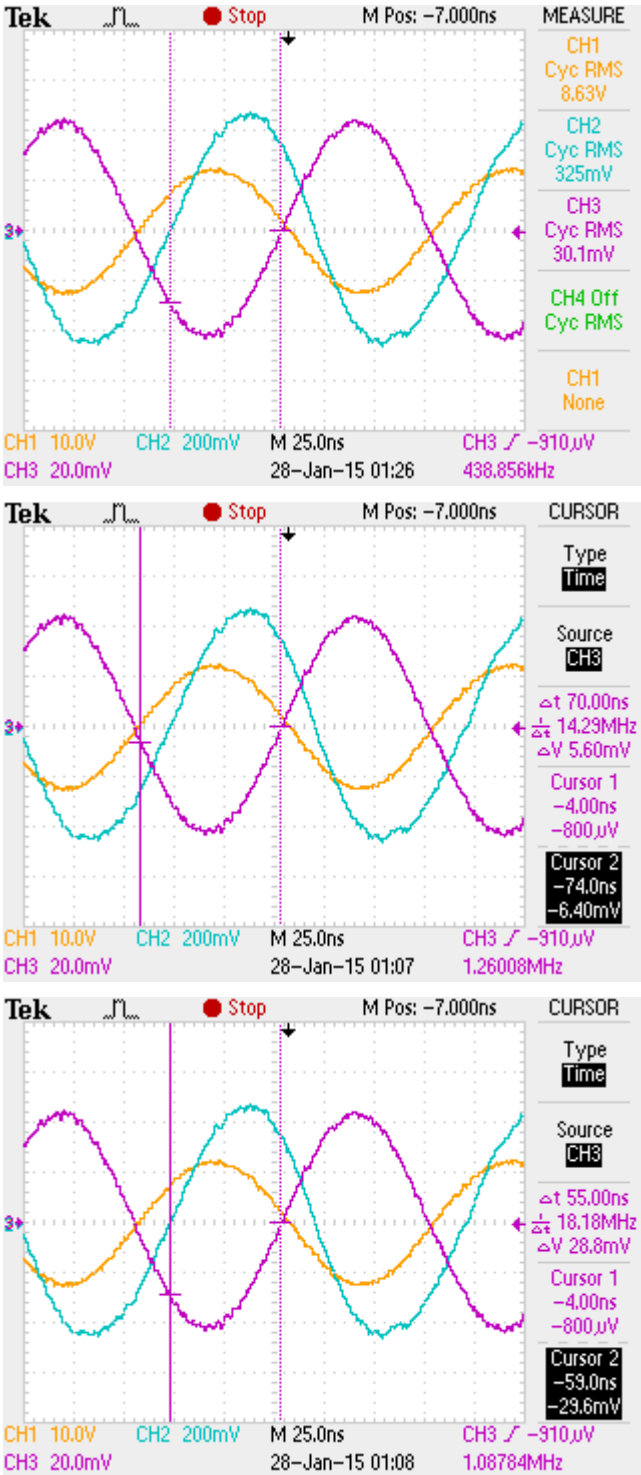

Channel 1 –Yellow = TC voltage

Channel 2 – Blue = TC current

Channel 3 – Purple = Model 100A B-Field probe voltage

Top Image - Voltage and Current Amplitudes

Middle Image - TC voltage phase difference relative to the B-Field probe

Bottom Image - TC current phase difference relative to the B-Field probe

Illustration 15: Oscilloscope images for centered configuration TC measurement with B-Field probe between TC and RNR. See column 3 of Table 7.

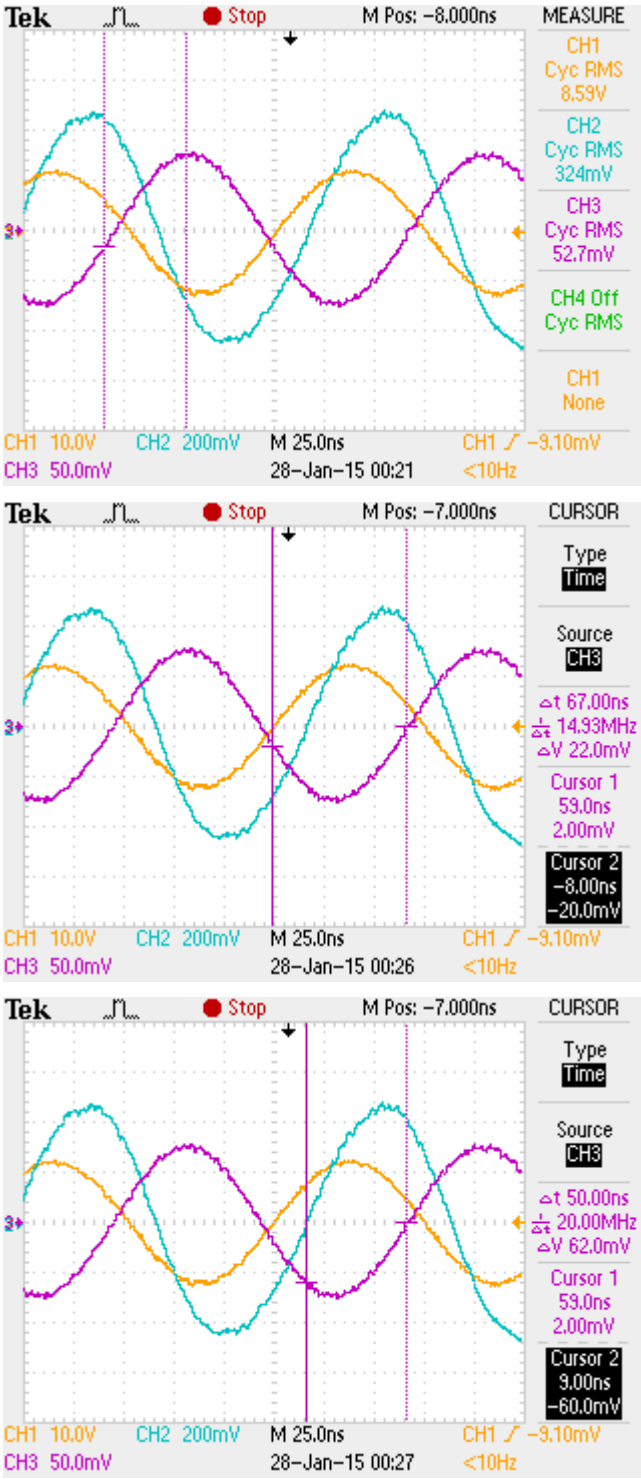

Channel 1 –Yellow = TC voltage

Channel 2 – Blue = TC current

Channel 3 – Purple = Model 100A B-Field probe voltage

Top Image - Voltage and Current Amplitudes

Middle Image - TC voltage phase difference relative to the B-Field probe

Bottom Image - TC current phase difference relative to the B-Field probe

Illustration 16: Oscilloscope images for centered configuration TC measurements and B-Field centered on TC. See column 2 of Table 7.

3.7 Offset Configuration

The summary results for the offset configuration current and voltage tests of the RNR are shown in Table 8. Corresponding oscilloscope images are shown in Illustration 17 and Illustration 18

Measurement Parameter	B-Field Probe on Transmit Coil	B-Field probe between TC and RNR
RNR Voltage	4.44V	4.56V
RNR Current	613mA	619mA
B-Field Probe Voltage	66.9mV	55.6mV
B-Field during RNR measurement	24.2uT	20.2uT
Time delay for RNR Voltage compared to B-Field	31.6ns	21.6ns
Time delay for RNR Current compared to B-Field	16.8ns	6.0ns

Table 8: Offset configuration results for RNR measurement.

The summary results for the offset configuration current and voltage tests on the TC are shown in Table 9. Corresponding oscilloscope images are shown in Illustration 19 and Illustration 20.

Measurement Parameter	B-Field Probe on Transmit Coil	B-Field probe between TC and RNR
Transmit Coil Voltage	10.0V	10.3V
Transmit Coil Current	284mA	284mA
Transmit Coil Input Power	2.84W	2.93W
B-Field Probe Voltage	66.5mV	55.4mV
B-Field during TC measurement	24.1uT	20.1uT
Time delay for TC Voltage compared to B-Field	-70ns	-79ns
Time delay for TC Current compared to B-Field	-52ns	-60ns
RNR Battery Charge Current	215mA	222mA

Table 9: Offset Configuration results for TC measurement.

As before, there is little difference between the B-field values when testing the RNR or TC provided the probe is fixed in the same location. Similarly, there is only a small change in measured voltage and current on either the RNR or TC with the probe in different locations. Again, this consistency suggests that the probe does not significantly perturb the coupling between the TC and RNR.

There is a modest difference in the B-field measurements at the different probe locations. This is expected and consistent with simulation as is shown in the next section.

All measurements are in RMS except for RNR battery charge current. All channels are AC coupled. Channel 3 is terminated in 50 ohms to facilitate power measurement from the B-field probe.

As can be seen in Table 9 above, the mobile charger regulates the power level delivered to the transmit coil to approximately 3 W RMS in all cases.

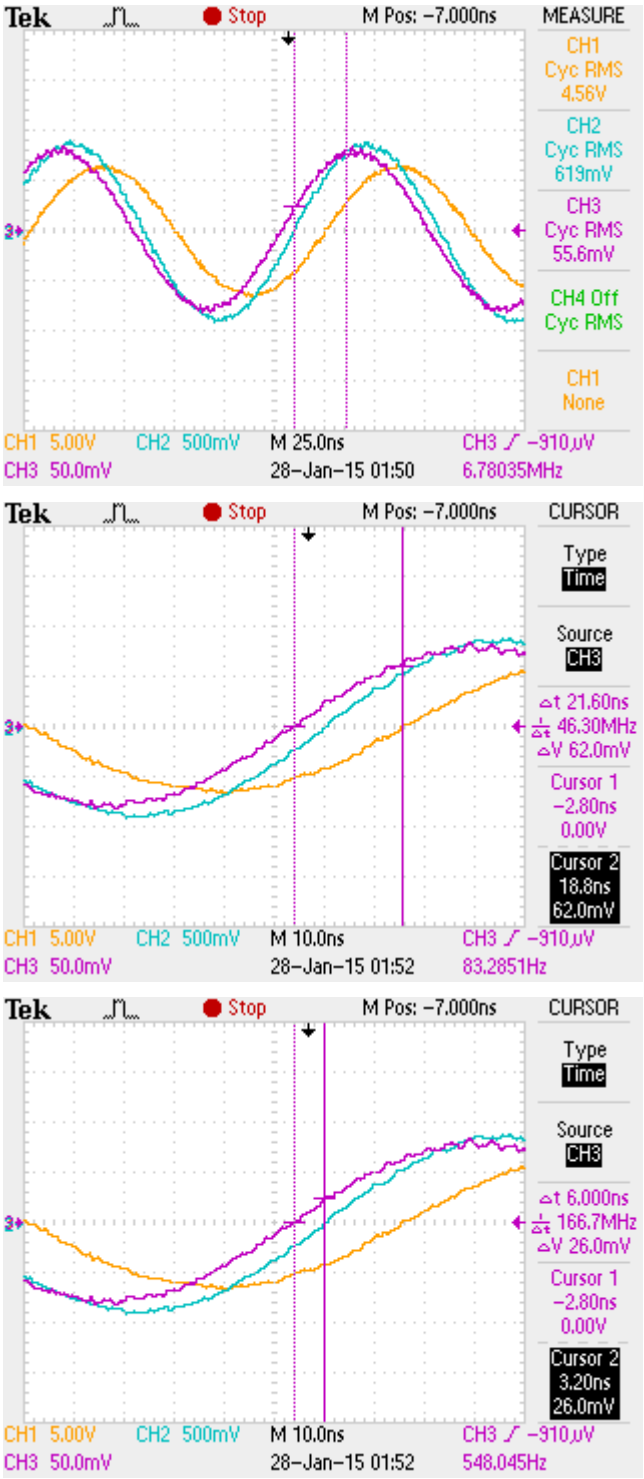

Channel 1 –Yellow = RNR tank voltage

Channel 2 – Blue = RNR current

Channel 3 – Purple = Model 100A B-Field probe voltage

Top Image - Voltage and Current Amplitudes

Middle Image - RNR tank voltage phase difference relative to the B-Field probe

Bottom Image - RNR current phase difference relative to the B-Field probe

Illustration 17: Oscilloscope images for offset configuration RNR tests with B-field probe centered between TC and RNR. See column 3 of Table 8.

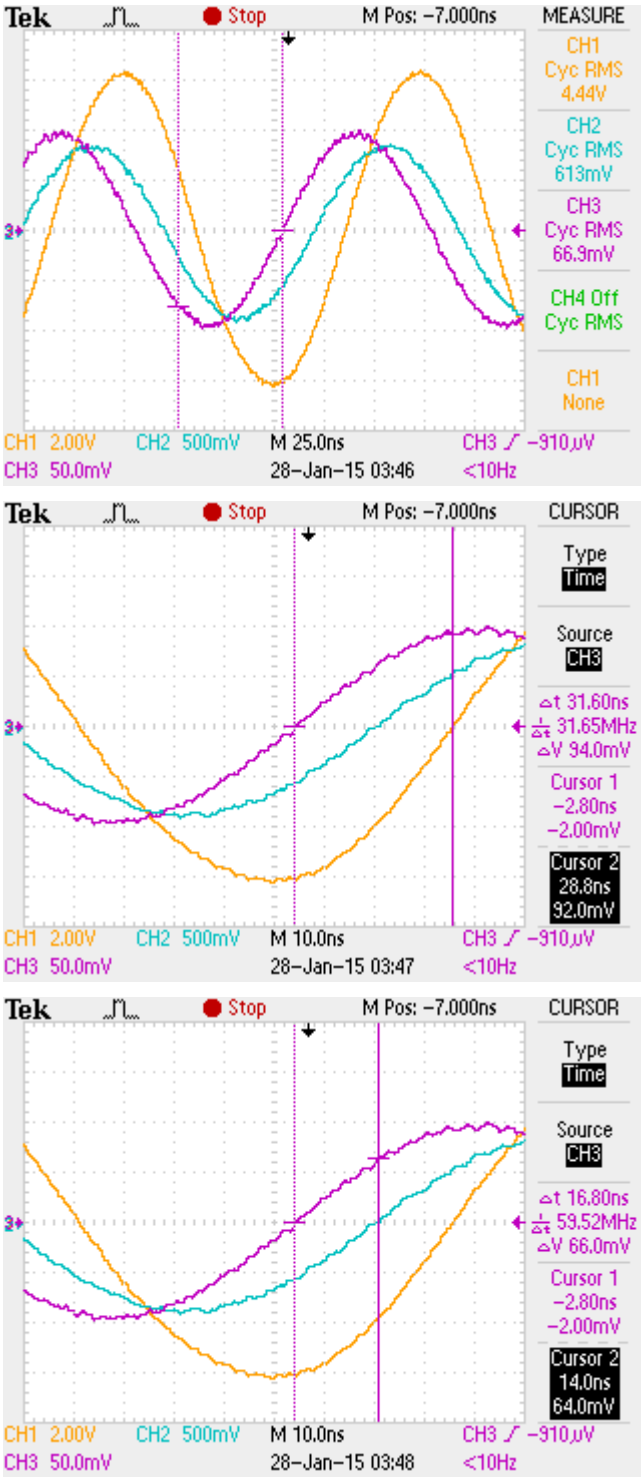

Channel 1 –Yellow = RNR tank voltage

Channel 2 – Blue = RNR current

Channel 3 – Purple = Model 100A B-Field probe voltage

Top Image - Voltage and Current Amplitudes

Middle Image - RNR tank voltage phase difference relative to the B-Field probe

Bottom Image - RNR current phase difference relative to the B-Field probe

Illustration 18: Oscilloscope images for offset configuration RNR tests with B-field probe centered on TC. See column 2 of Table 8.

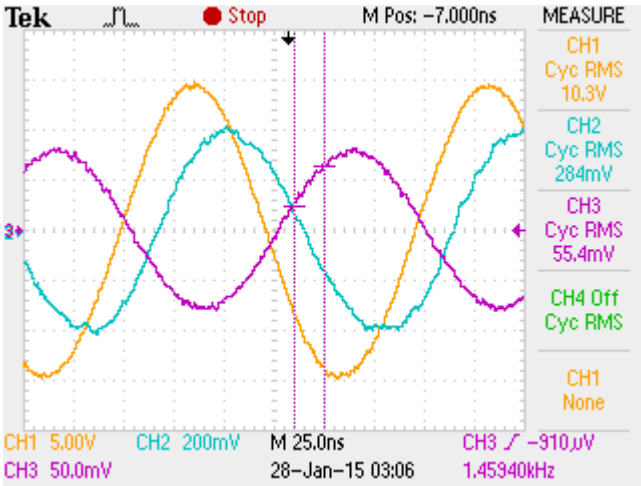

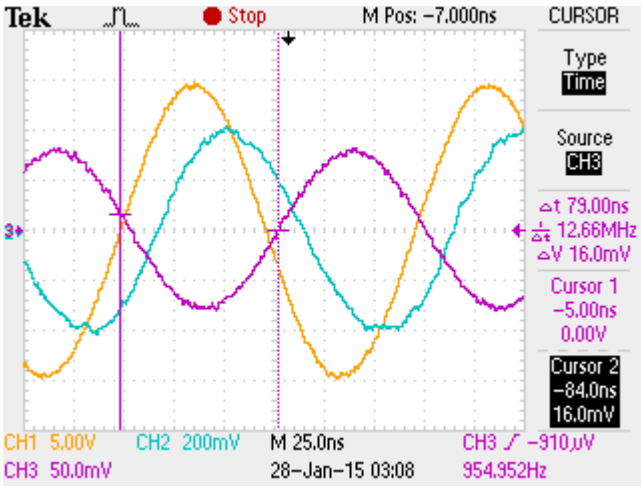

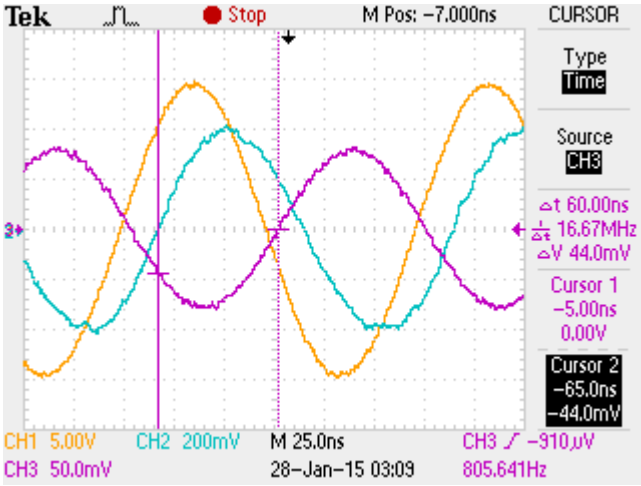

Channel 1 –Yellow = TC voltage

Channel 2 – Blue = TC current

Channel 3 – Purple = Model 100A B-Field probe voltage

Top Image - Voltage and Current Amplitudes

Middle Image - TC voltage phase difference relative to the B-Field probe

Bottom Image - TC current phase difference relative to the B-Field probe

Illustration 19: Oscilloscope images for offset configuration TC tests with B-field probe between RNR and TC. See column 3 of Table 9.

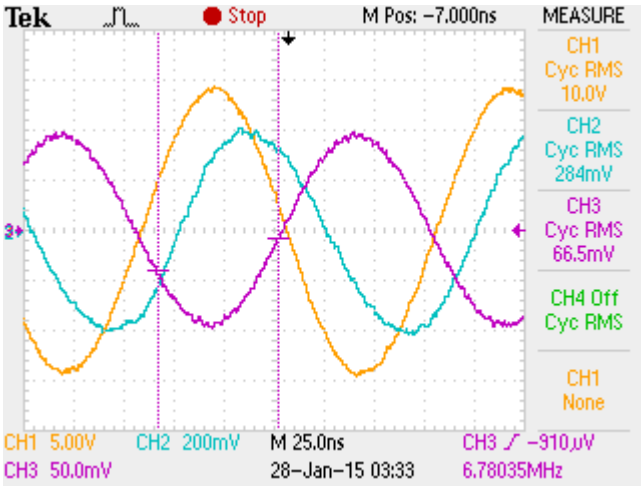

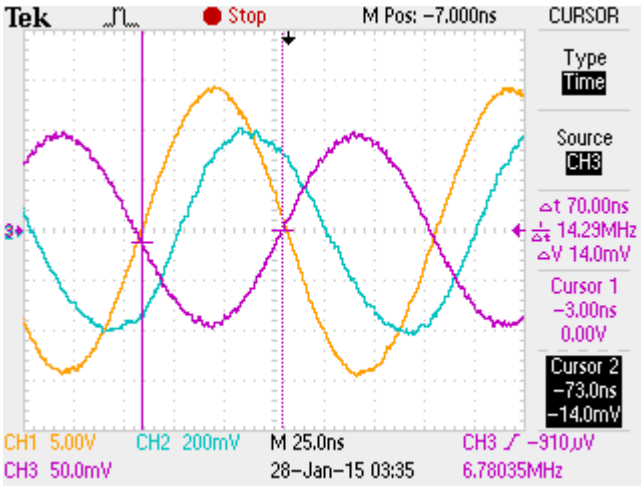

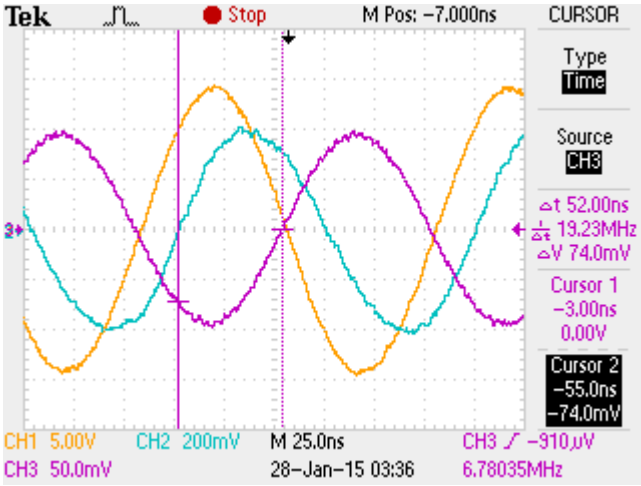

Channel 1 –Yellow = TC voltage

Channel 2 – Blue = TC current

Channel 3 – Purple = Model 100A B-Field probe voltage

Top Image - Voltage and Current Amplitudes

Middle Image - TC voltage phase difference relative to the B-Field probe

Bottom Image - TC current phase difference relative to the B-Field probe

Illustration 20: Oscilloscope images for offset configuration TC tests with B-field probe centered on TC. See column 2 of Table 9.

4 Spice Simulation and Source Modeling

The work in this section was carried out by Mr. Weijand. This section is an edited version of his internal report.

The circuit modeling was carried out using the well known and highly regarded Linear Technologies LTSpice IV simulator. The measured results from the previous section along with known time delays of the cables and probes were used derive the equivalent current source magnitude and phase to be injected into the TC and RNR coils in the Remcom field simulator. The additional laboratory data that was made available for this report greatly simplified the circuit modeling effort as compared to the work shown in the previous iteration of this report. The previous discussion is therefore no longer relevant and not included here.

4.1 Centered Configuration Analysis

4.1.1 TC coil current derivation

The current injected into the resonating tank and voltage of a capacitor of the tank are measured and the phase relationships determined. Referring to the circuit model shown in Illustration 21, the tank circuit is replaced by a voltage source of the same amplitude and phase as measured on the capacitor. The current source I1 represents the current measured as driven from the transmitter. Voltage source V1 is the voltage on the capacitor at the end of the test cable. The actual current in the coil is the current flowing through V1. This model is an application of the Kirchhoff current law.

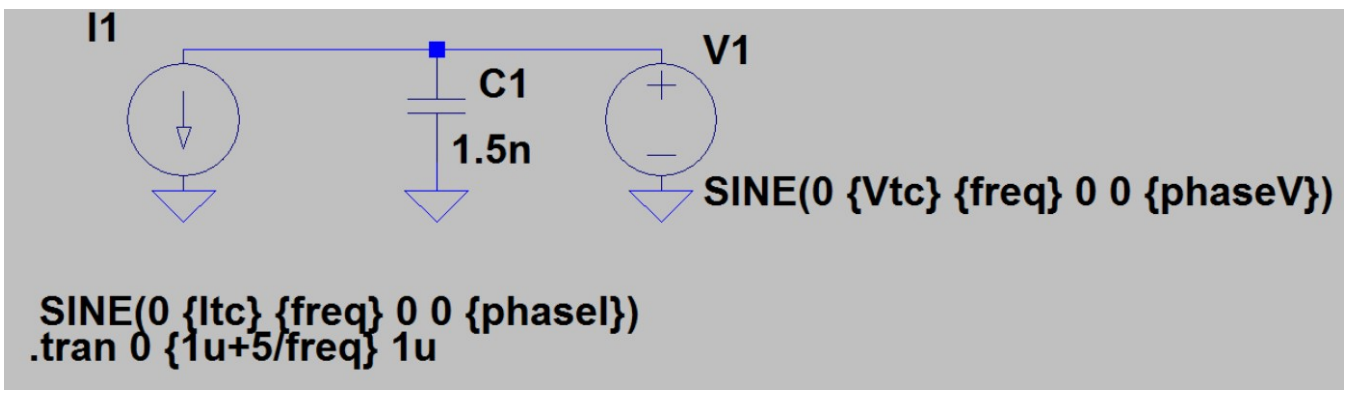

Illustration 21: LT-Spice schematic diagram.

4.1.2 Current probe , voltage probe and cable delay corrections

The current probe, including the cable, has a known time delay of 20ns. The oscilloscope scope probe is 42 inches long and has a known cable delay of 5ns. The current of the TC system is measured at the connector. The transmit coil current delay due to 2 feet of transmit coil cable is calculated as 2.2nsec.

4.1.3 Calculations and measurements

The B-field probe voltage was used as a reference signal for timing. The timing information shown in Table 10 was derived from the oscilloscope images shown in Illustration 15.

Transmit Coil Current	
B-field to TC current delta	-55 ns
B-field probe delay	-20 ns
TC current delay due to TC cable length (measured at connector, delay to coil)	2.2 ns
Total Delay	**-72.8 ns**
Transmit Coil Voltage	
B-field probe to TC Voltage delta	-70 ns
Scope Probe Delay	-5 ns
Total Delay	**-75 ns**
Net Time Difference (-75ns-(-72.8ns))	**-2.2 ns**
Phase Angle Equivalent at 6.78 MHz	**-5.4 degrees**

Table 10: Centered configuration timing information.

4.1.4 Kirchhoff's Law simulation

Refer to the schematic of Illustration 21 for the meaning of LTSpice parameters. The time delay between TC voltage and TC current of 2.2ns corresponds to a phase angle of ~5 degrees of phase at the operating frequency of 6.78 MHz (***freq*** parameter). This is an angle of 175 degrees (***phaseI*** parameter), since the the current source direction in the schematic is opposite that of the actual measurement. Extracting values from the oscilloscope images of Illustration 15 result in the amplitude values shown in Table 11. The current amplitude is taken from the probe current amplitude (325mA RMS) and converted to peak (***Itc*** parameter). The voltage amplitude is taken from the scope TC coil voltage measurement (8.63V RMS) and converted to peak (***Vtc*** parameter).

Parameter	RMS Values	Peak Values
Voltage, V, V	8.63	12.2
Current, I, mA	325	460

Table 11: RMS and Peak values of circuit model parameters.

The derived values are entered into the LTSpice simulator using a ***.param*** statement;

.param Itc=0.46 freq=6.78e6 phaseI=175 Vtc=12.2 phaseV=0

The result ***tdelta*** is determined using the .measure statement to determine the relative time of zero crossings of the capacitor voltage, ***V(n001)***, and the current, ***I(V1)***, through the antenna represented by the voltage source, ***V1***. The ***.measure*** statements are as follows:

.measure tran t0drive WHEN v(n001)=0 rise=1 TD=210ns
.measure tran t0L1 WHEN I(V1)=0 rise=1 TD=210ns
.measure tran tdelta param t0L1-t0drive

The corresponding values reported in the LTSpice log file are as follows:

t0drive: v(n001)=0 AT 3.27434e-007
t0l1: i(v1)=0 AT 3.52344e-007
tdelta: t0l1-t0drive=2.49108e-008

The LTSpice graphical tool output shown in Illustration 22 is used to determine the actual antenna coil current of 663mA RMS (937.6mA peak). The simulation is set to run exactly 5 cycles, as demonstrated by the very small average current value of -229nA.

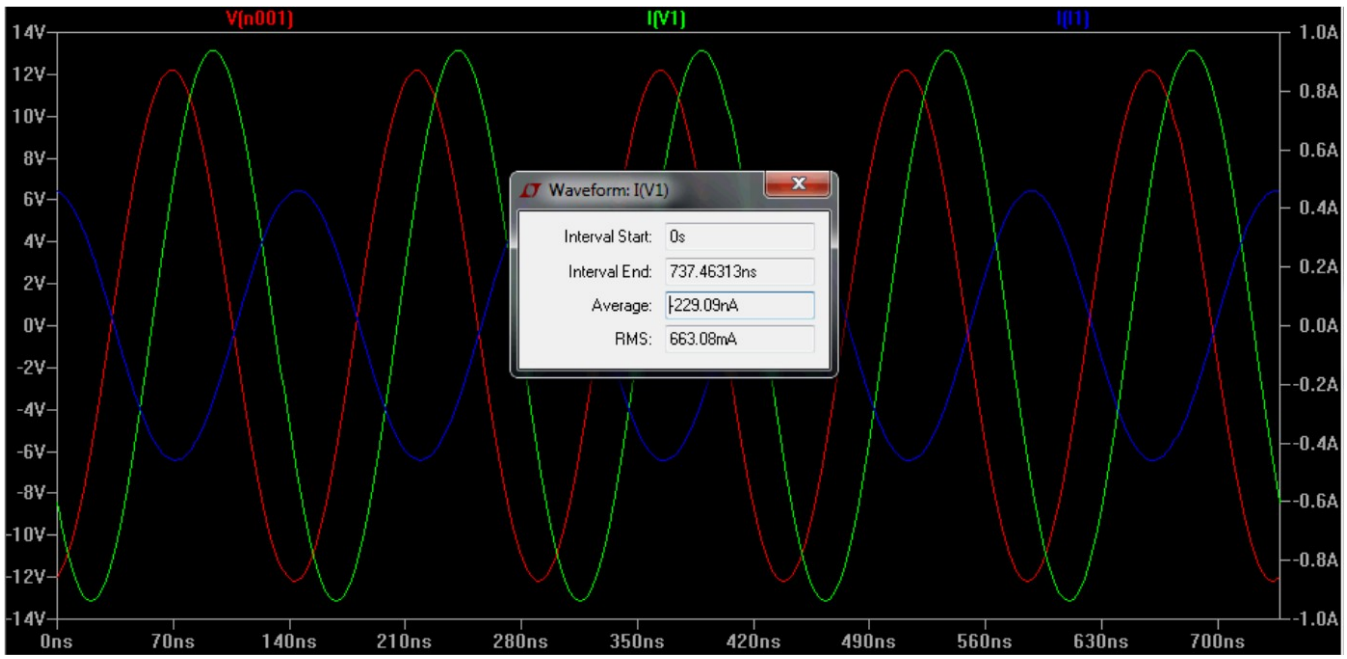

Illustration 22: LTSpice computed waveforms for centered configuration.

The TC coil current angle is measured relative to the tank voltage and the tank voltage is leading the current by ***tdelta*** of 25 ns, (rounded off from 2.49108e-8). The tank voltage is leading the B-field zero reference by 75ns (or 2ns half cycle opposite polarity), thus the B-field is lagging the coil current by (75ns-25ns) = 50ns. This value will be used in the result section.

4.1.5 RNR coil current phase

The RNR coil current phase and amplitude are derived from the oscilloscope images of Illustration 13. As seen in the illustrations, the current is lagging the B-field reference signal by 10.4ns. Accounting for the 20ns probe delay, the current is leading the B-field signal by 9.6ns. The RNR current is measured to be be 633mA RMS using a (1 A/V) conversion factor for the current probe.

4.1.6 Centered Configuration Source Condition Summary

The TC coil is leading the RNR current by the sum of (50 – 9.6) ns = 40.4ns. This time delay is equivalent to a phase angle of 98 degrees at the operating frequency of 6.78 MHz. The TC coil amplitude is 663mA RMS (937.6mA peak) and the RNR coil amplitude is 633mA RMS (895.2mA peak).

4.2 Offset Configuration Analysis

4.2.1 TC coil current derivation

The current injected into the resonating tank and voltage of a capacitor of the tank are measured and the phase relationships determined. Referring to the circuit model shown in Illustration 23, the tank circuit is replaced by a voltage source of the same amplitude and phase as measured on the capacitor. The current source I1 represents the current measured as driven from the transmitter. Voltage source V1 is the voltage on the capacitor at the end of the test cable. The actual current in the coil is the current flowing through V1. This model is an application of the Kirchhoff current law.

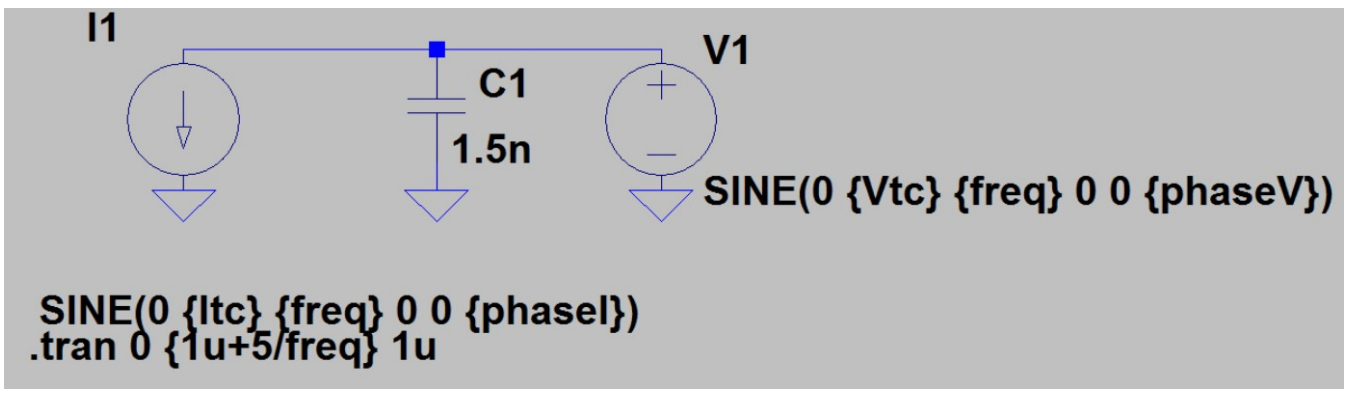

Illustration 23: LT-Spice schematic diagram.

4.2.2 Current probe , voltage probe and cable delay corrections

The current probe, including the cable, has a known time delay of 20ns. The oscilloscope scope probe is 42 inches long and has a known cable delay of 5ns. The current of the TC system is measured at the connector. The transmit coil current delay due to 2 feet of transmit coil cable is calculated as 2.2nsec.

4.2.3 Calculations and Measurements

The B-field probe voltage was used as a reference signal timing signal and the timing information shown in Table 12 was derived from the oscilloscope images shown in Illustration 19.

Transmit Coil Current	
B-field probe to TC current delta	-60 ns
B-field probe delay	-20 ns
TC current delay due to TC cable length (measured at connector delay to coil)	2.2 ns
Total	**-77.8 ns**
Transmit Coil Voltage	
B-field probe to TC voltage delta	-79 ns
Scope probe delay	-5 ns
Total Delay	**-84 ns**
Time Difference (-84 ns- (-77.8 ns))	**-6.2 ns**
Equivalent Phase Angle at 6.78 MHz	**-15 degrees**

Table 12: Offset configuration timing information

4.2.4 Kirchhoff's Law simulation

Refer to the schematic of Illustration 23 for the meaning of LTSpice parameters. The time delay between TC voltage and cable current of 6.2ns corresponds to a phase angle of ~15 degrees of phase at the operating frequency of 6.78 MHz (***freq*** parameter). This is an angle of 165 degrees (***phaseI*** parameter), since the current source direction in the schematic is opposite of the actual measurement. Extracting values from the oscilloscope images of Illustration 19 results the values shown in Table 13. The current amplitude is taken from the probe current amplitude (284mA RMS) and converted to peak (***Itc*** parameter). The voltage amplitude is taken from the scope TC coil voltage measurement (10.3V RMS) and converted to peak (***Vtc*** parameter).

Parameter	RMS Values	Peak Values
Voltage, V, Volts	10.3	14.57
Current, I, mA	284	401

Table 13: RMS and Peak values of circuit model parameters.

The derived values are entered into the LTSpice simulator as a ***.param*** statement:

.param Itc=0.401 freq=6.78e6 phaseI=165 Vtc=14.57 phaseV=0

The result tdelta is determined using the .measure statement to determine the relative time of zero crossings of the capacitor voltage, ***V(n001)***, and the current, ***I(V1)***, through the antenna represented by the voltage source, ***V1***. The ***.measure*** statements are as follows:

.measure tran t0drive WHEN v(n001)=0 rise=1 TD=210n
.measure tran t0L1 WHEN I(V1)=0 rise=1 TD=210n
.measure tran tdelta param t0L1-t0drive

The corresponding values reported in the LTSpice log file are as follows:

t0drive: v(n001)=0 AT 3.27434e-007
t0l1: i(v1)=0 AT 3.5592e-007
tdelta: t0l1-t0drive=2.8486e-008

The LTSpice graphical tool output shown in Illustration 24 is used to determine the actual antenna coil current of 779.8mA RMS (1102.8mA peak). The simulation is set to run exactly 5 cycles, as demonstrated by the very small average current value of -307.54nA.

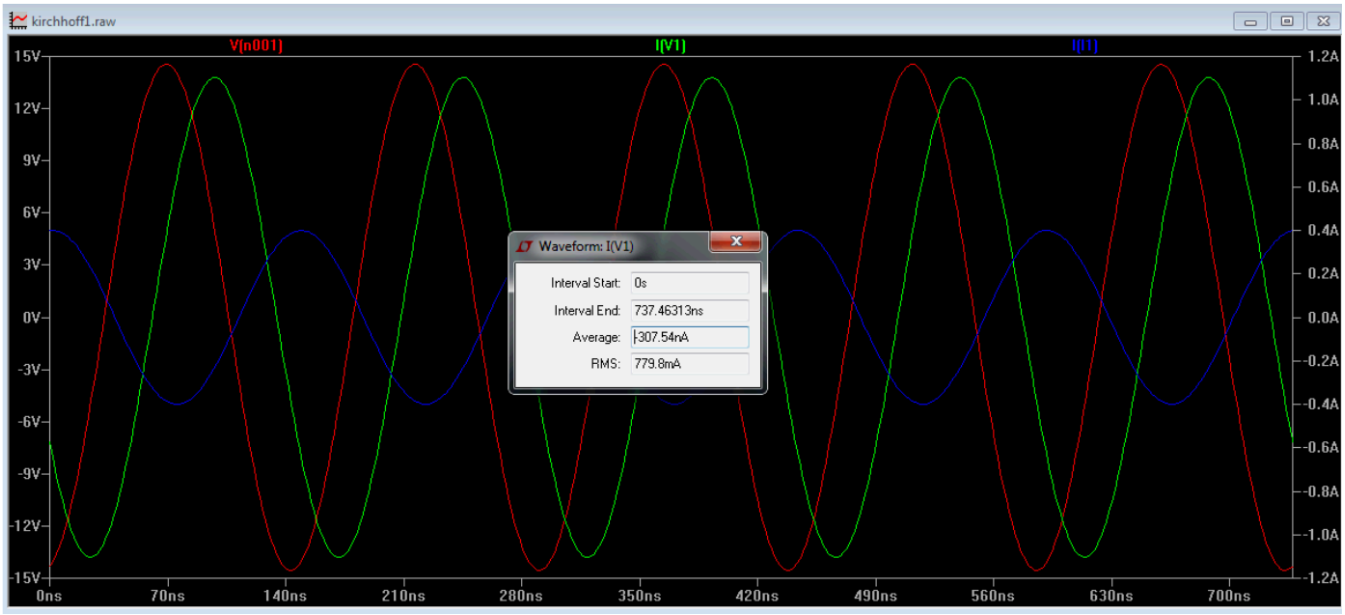

Illustration 24: LTSpice computed waveforms for offset configuration.

The TC coil current angle is measured relative to the tank voltage and the tank voltage is leading the current by ***tdelta*** of 29 ns, (rounded off from 2.8486e-8s).

The tank voltage is leading the B-field zero reference by 84ns (or 11ns half cycle opposite polarity), thus the B-field is lagging the coil current by (84-29)ns = 55ns. This value will be used in the result section.

The voltage source current is measured in the simulation and is 779.8mA RMS. This is the value of the current in the transmit coil. Note: Due to a transposition error a value of 790mA RMS (1117.2mA peak) was inadvertently used in the simulations. This error results in approximately 1.3% over estimate in the current of the TC coil current. An error of this magnitude is relatively small given the other assumptions used in this analysis so the lengthy simulations were not repeated with the lower value.

4.2.5 RNR coil current phase

The RNR coil current phase and amplitude are derived from the oscilloscope images of Illustration 17. As seen in the illustrations, the current is lagging the B-field reference signal by 6ns minus 20ns probe delay = 14ns leading the B-field. The RNR current is measured to be be 619mA RMS using a (1 A/V) conversion factor for the current probe.

4.2.6 Offset Configuration Source Condition Summary

The TC coil is leading the RNR current by (55 – 14) ns = 41ns. This time delay is equivalent to a phase angle of 100 degrees at the operating frequency of 6.78 MHz.

The TC coil amplitude is 790mA RMS (1117.2mA peak) and the RNR coil amplitude is 619mA RMS (875.4mA peak).

5 Field Simulation and Validation

This section summarizes the simulator current, voltage and field results for the centered and offset configurations. Computed B-field values are seen to agree with measured B-field values at several points in the simulation space.

5.1 Centered Configuration

The centered configuration is the nominal configuration and represents typical device operation. A top view of the CAD model for this case is shown in Illustration 25. A side view is shown in Illustration 26.

As shown in the illustrations, the bottom surface of the transmit coil silicone covering is flush with the top face of the body phantom slab. The transmit coil is approximately centered laterally in the solution space. Excepting the silicone region forming the coaxial feed cable stress relief, the shortest distance from the edge of the transmit coil covering to a boundary face is approximately 27 mm.

The top face of the RNR is located approximately 25 mm below the top face of the body phantom. This is the recommended implant depth for the device. The bottom face of the RNR device is thus located approximately 33 mm above the bottom face of the body phantom slab. The RNR is slightly offset from lateral center and the shortest lateral distance from a side face of the RNR device to the boundary of the body phantom is approximately 42 mm.

The above mentioned distances to boundaries do NOT include PML (Perfectly Matched Layers).

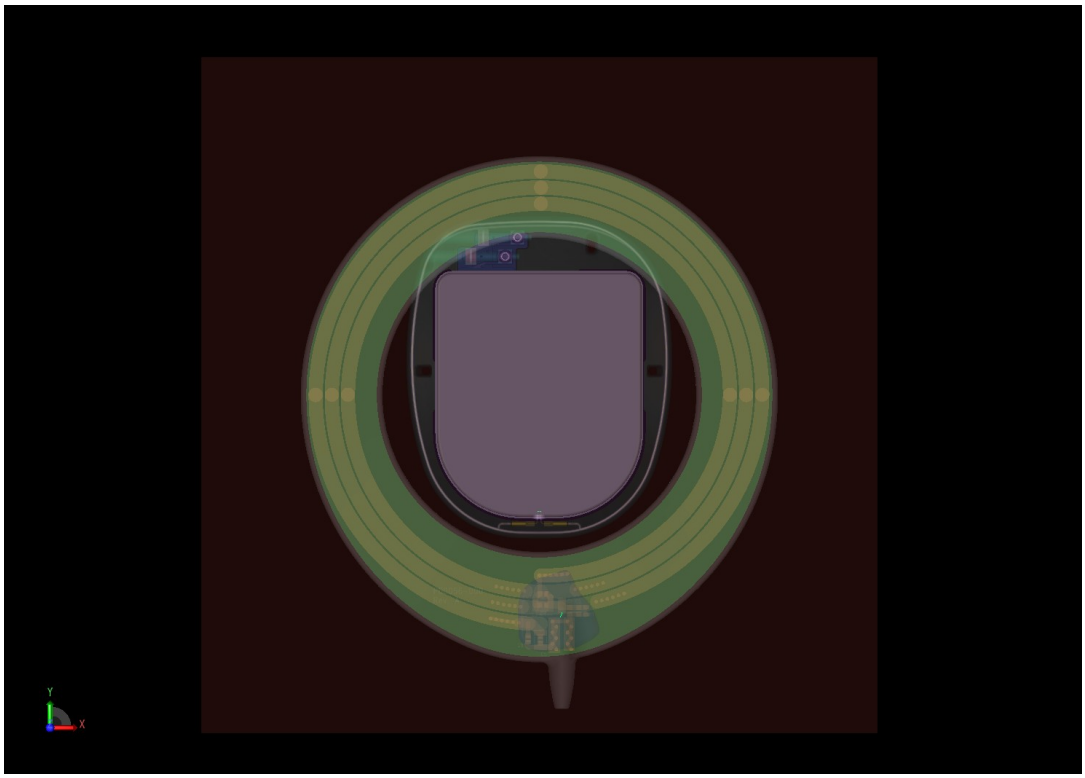

Illustration 25: Top view of centered configuration.

Illustration 26: Side view of centered configuration.

5.1.1 Simulation Diagnostics

The Remcom simulator was configured to run a minimum of two and a maximum of four oscillations of the 6.78 MHz sinusoid. The workstation was configured to run using all available cores (1792 CUDA cores and 8 CPU cores) and required approximately 30.75 hours to compute the steady state fields. The solution reached a convergence value of -35.17 dB which is generally considered acceptable for a steady state solution. An additional 8.75 hours was required to compute the 1 gram and 10 gram SAR averages.

5.1.2 Computed Current and Voltage Waveforms

As shown in the previous section, the source condition for the TC is 937.6 mA peak at 0 degrees phase. The source condition for the RNR is 895.2 mA peak at -98 degrees phase.

A plot of computed current through the TC and RNR is shown in Illustration 27. The TC current (blue) is sinusoidal with peaks of approximately 855.5mA. The peak amplitude is approximately 8.5% lower than the source condition. This is most likely due to differences in the coupling factor between the coils in the measurement versus simulation. The RNR current (red) exhibits a turn on transient that dies off within about 1 cycle. Afterward it is sinusoidal with peaks of 895.4mA. The agreement with RNR source condition is excellent.

A plot of the computed voltage at the TC and RNR source terminals is shown in Illustration 28. The TC source voltage (blue) is sinusoidal with peaks approximately 87.7V. The RNR coil voltage (red) exhibits a turn on transient that dies out within about 1 cycle. Afterwards, the waveform is sinusoidal with peaks of approximately 63.7V. These values are consistent with the design values of the device.

The Remcom solver was configured to record only steady state fields (as opposed to transient fields) so the effects of the transient currents and voltages shown above are not included in the field plots or SAR calculations shown in the next section.

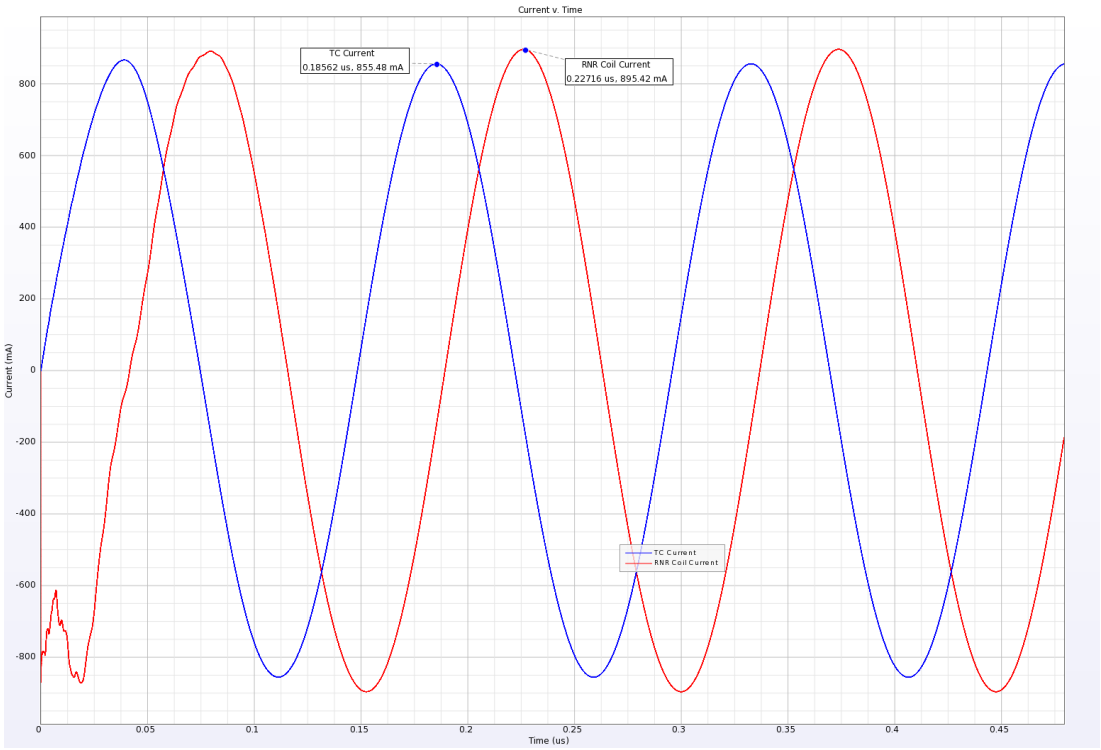

Illustration 27: Computed current in TC and RNR coil.

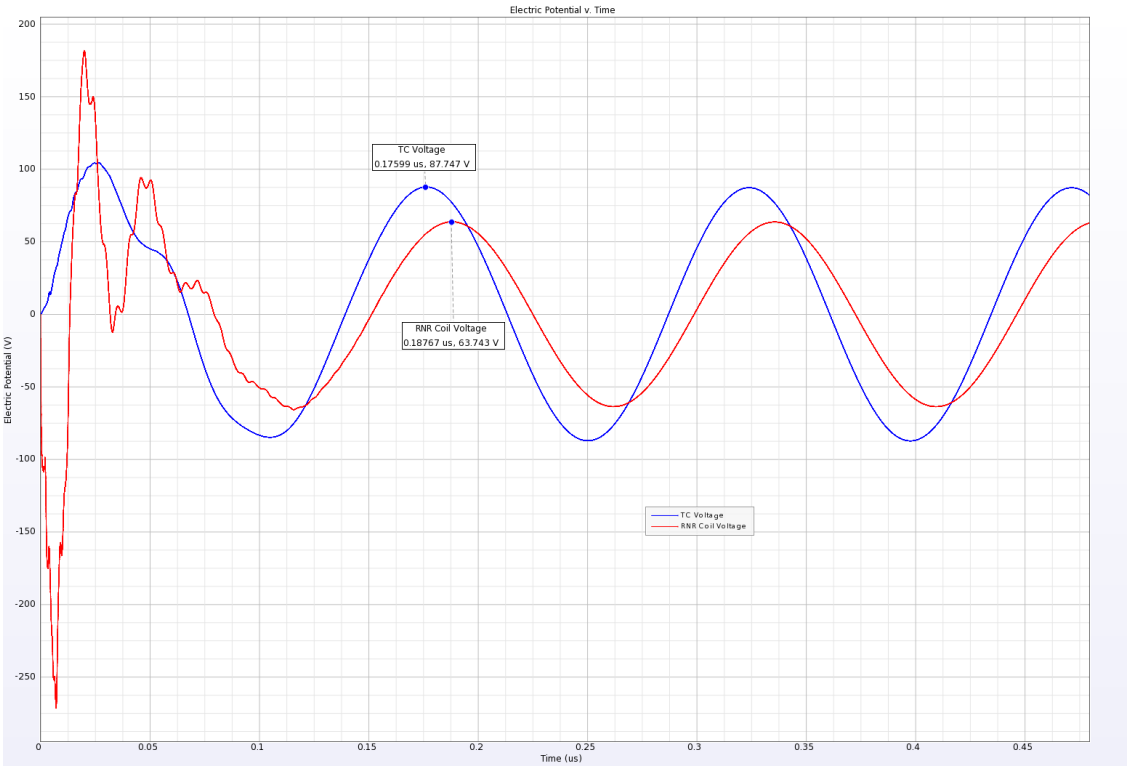

Illustration 28: Computed voltage at terminals of TC and RNR coil

5.1.3 Computed B-fields

Centered Probe on TC

A plot of the z-component of computed B-field (uT) in a horizontal slice taken just above (+1mm) the plane of the TC is shown in Illustration 29. Color scale is linear and normalized to 50uT. Red regions can exceed normalization value. Phase angle is 110 degrees. The B-field at the pointer location is ~28.7uT peak (20.3uT RMS). Field gradient is clearly small in this region so probe averaging effects should be minimal.

Centered Probe between TC and RNR

A plot of the z-component of computed B-field (uT) in a horizontal slice taken midway between the TC and RNR (z=-12.7358mm) is shown in Illustration 30. Color scale is linear and normalized to 50uT. Red regions can exceed normalization value. Phase angle is 120 degrees. The B-field at the pointer location is ~17.5uT peak (12.4uT RMS). Again field gradient is small so probe averaging effects should be minimal.

Comparison to Measurement

A summary of the the B-field probe measurements and B-field computations is shown in Table 14. Measured values represent the average of data taken when testing the TC and RNR coil. Computations are peak values near center of probe location and do not account for probe averaging. The simulations over estimate field strength by as much as 12.7% in the location between the TC and RNR.

Location	Measured B-field (uT)	Computed B-field (uT)
TC centered, z=+1mm	19	20.3
TC centered, z=-12.7mm	11	12.4

Table 14: Measured versus computed B-field for centered configuration.

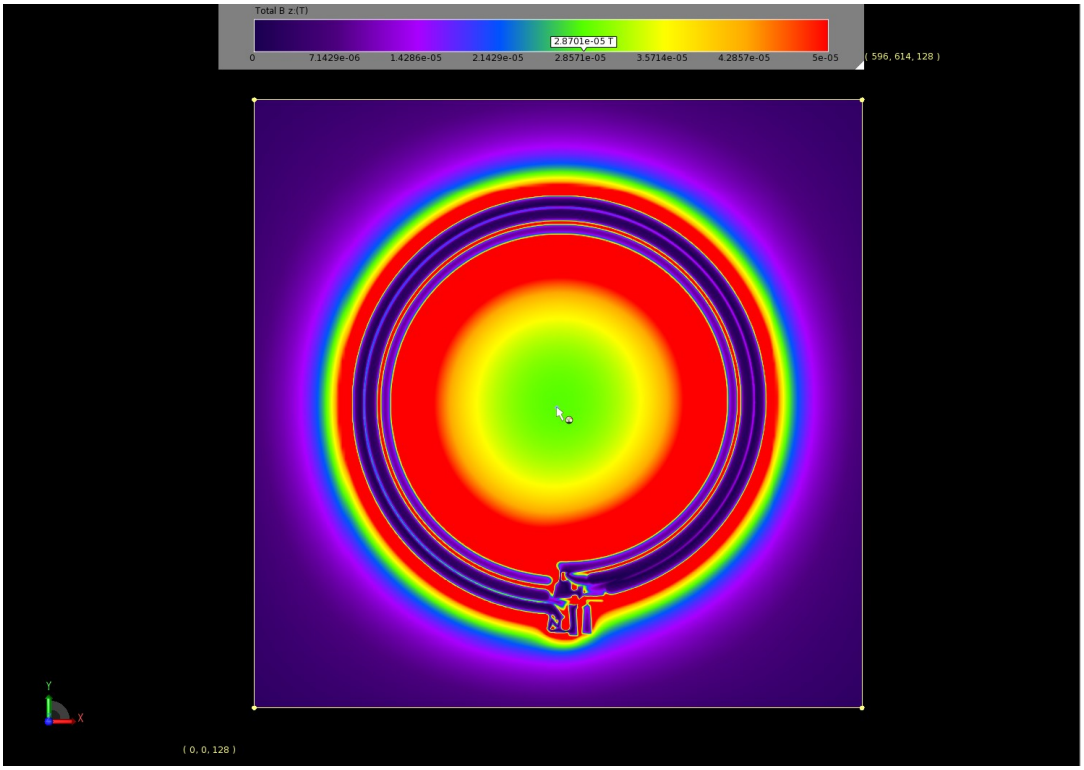

Illustration 29: Centered configuration B-field slice in plane of TC.

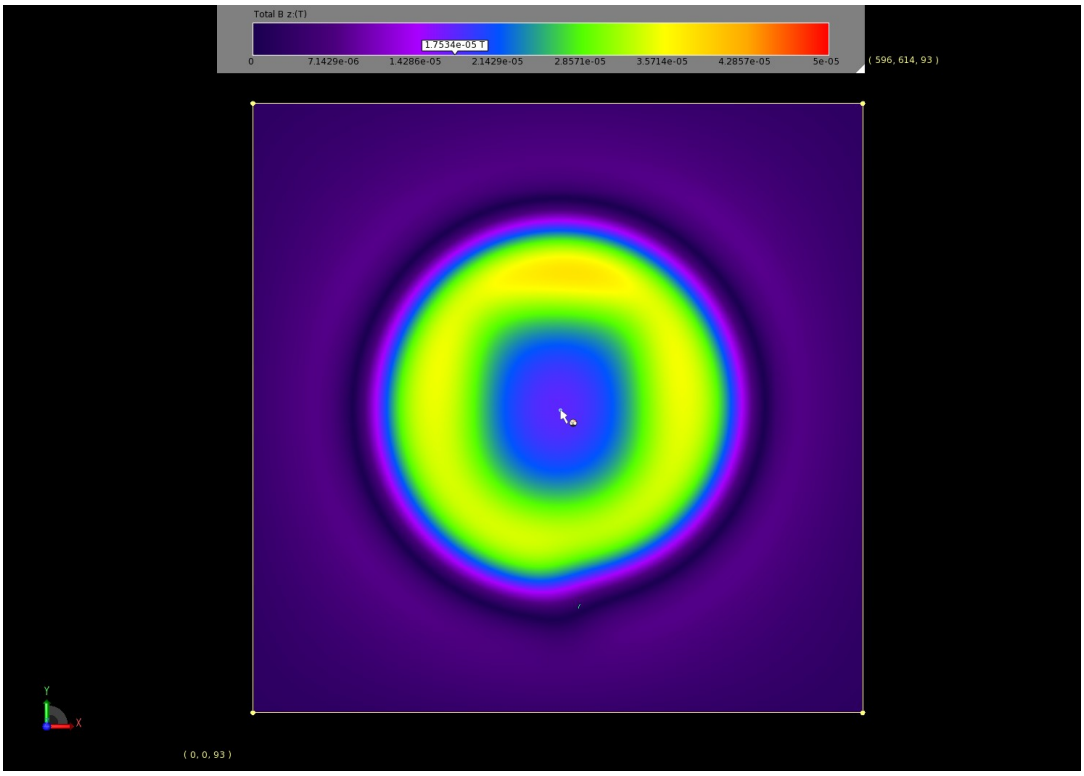

Illustration 30: Centered configuration B-field midway between TC and RNR.

5.1.4 Additional H-Field and E-Field plots

A false color plot of the computed H-field (A/m) (vector magnitude) in a vertical slice taken through the approximate center of the simulation space is shown in Illustration 31. Color scale is in dB and normalized to 1000 A/m. Red regions can exceed normalization value. This particular image is for 0 phase and shows weak H-fields near the TC and stronger fields near the RNR coil. The plot of Illustration 32 (same scale) shows the same vertical slice at 100 degree phase angle. Here, the fields are much stronger near the TC and weaker near the RNR coil.

A false color plot of the computed E-field (V/m) (vector magnitude) in the same vertical slice is shown in Illustration 33. Color scale is in dB and normalized to 10,000 V/m. Red regions can exceed normalization value. The zero phase plot shows that the E-field levels are maximum inside the TC and near the windings of the RNR coil. Maximum field values are reached in non-tissue media. The fields decay extremely rapidly with distance from the transmit and RNR coils. Field values in most of the tissue region are many orders of magnitude lower than values computed in the tissue phantom. The plot for 100 degree phase is shown in Illustration 34 (same scale) and again shows that peak values are generally limited to non-tissue regions and that they decay very rapidly with distance.

It should be noted that there E and H field plots do not show any indication of extraneous reflections from the absorbing boundary layers imposed on the tissue slab surfaces (not including top where the coil is placed). This efficiency of the absorbing boundary condition is critical to ensure the validity of the FDTD solution.

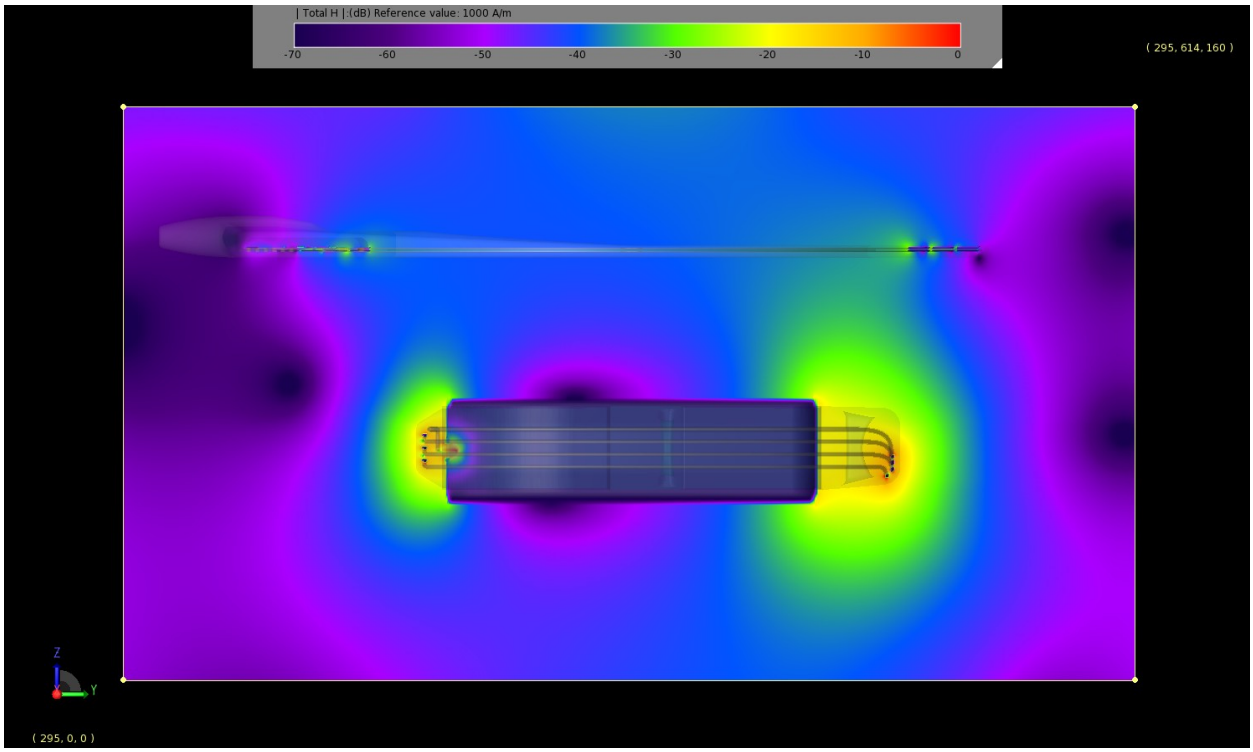

Illustration 31: Vertical slice computed H-Field at 0 degrees phase. Normalized to 1,000 A/m.

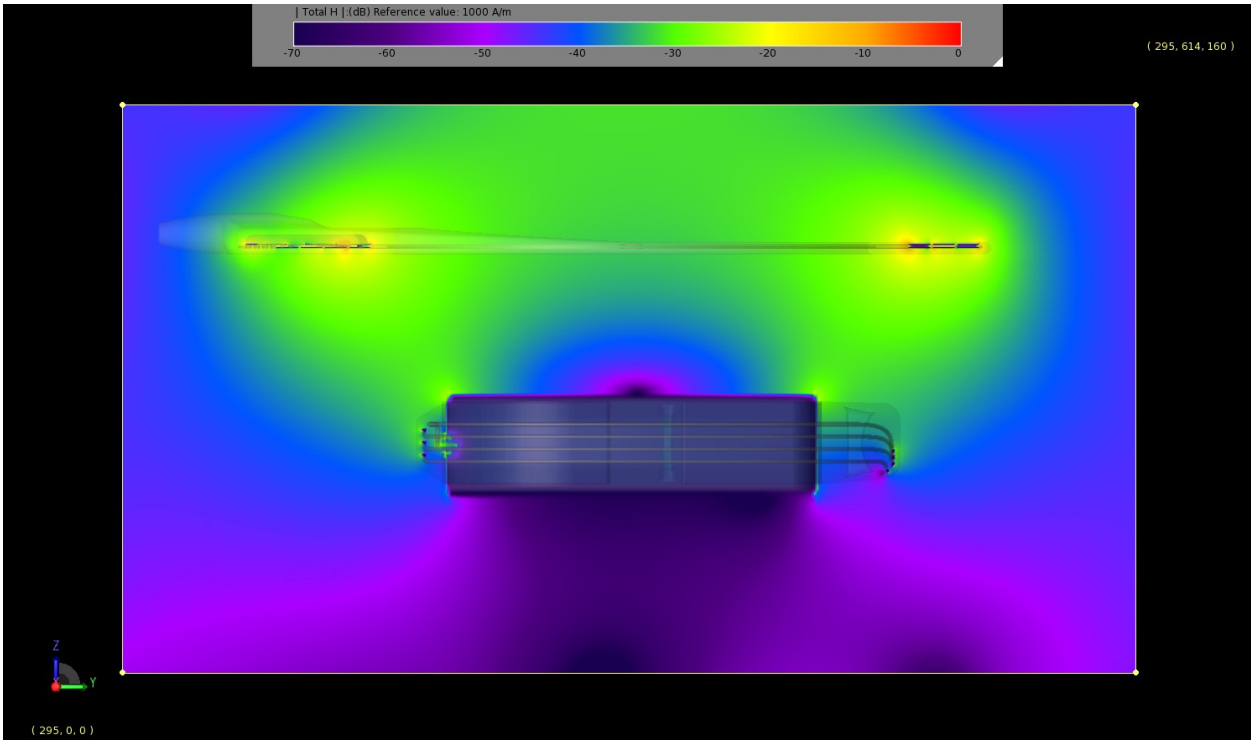

Illustration 32: Vertical slice computed H-Field at 100 degrees phase. Normalized to 1,000 A/m.

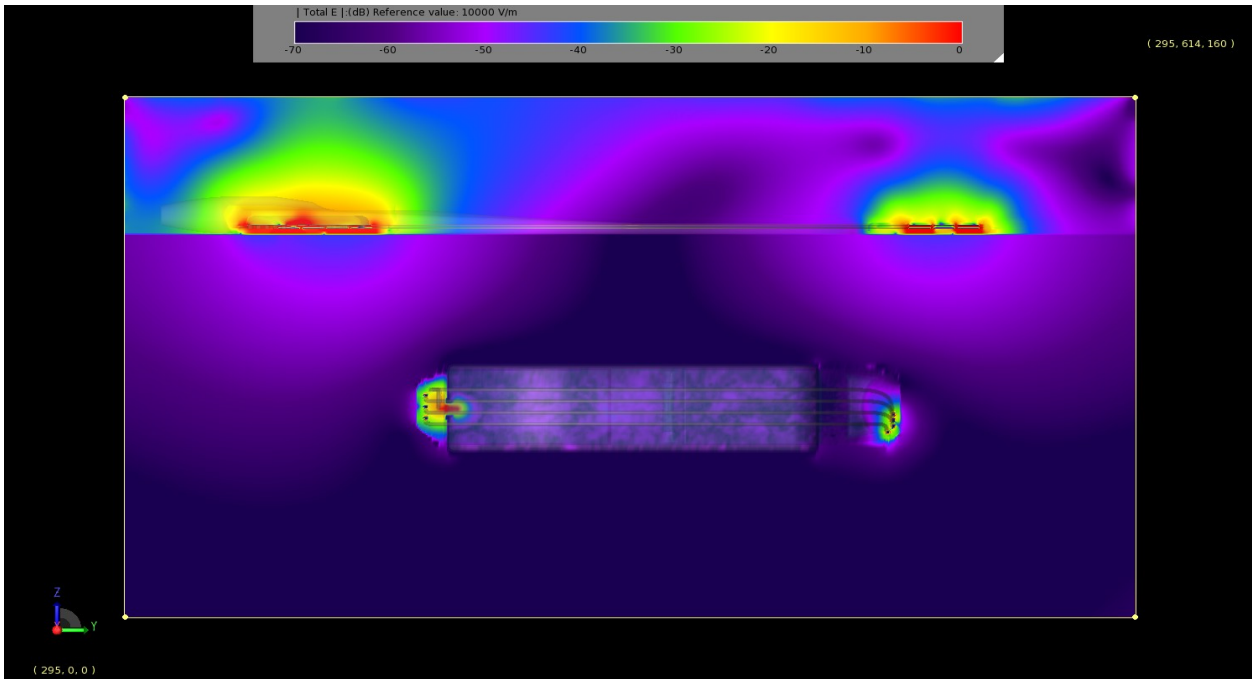

Illustration 33: Vertical slice computed E-field at 0 degrees phase. Normalized to 10,000 V/m.

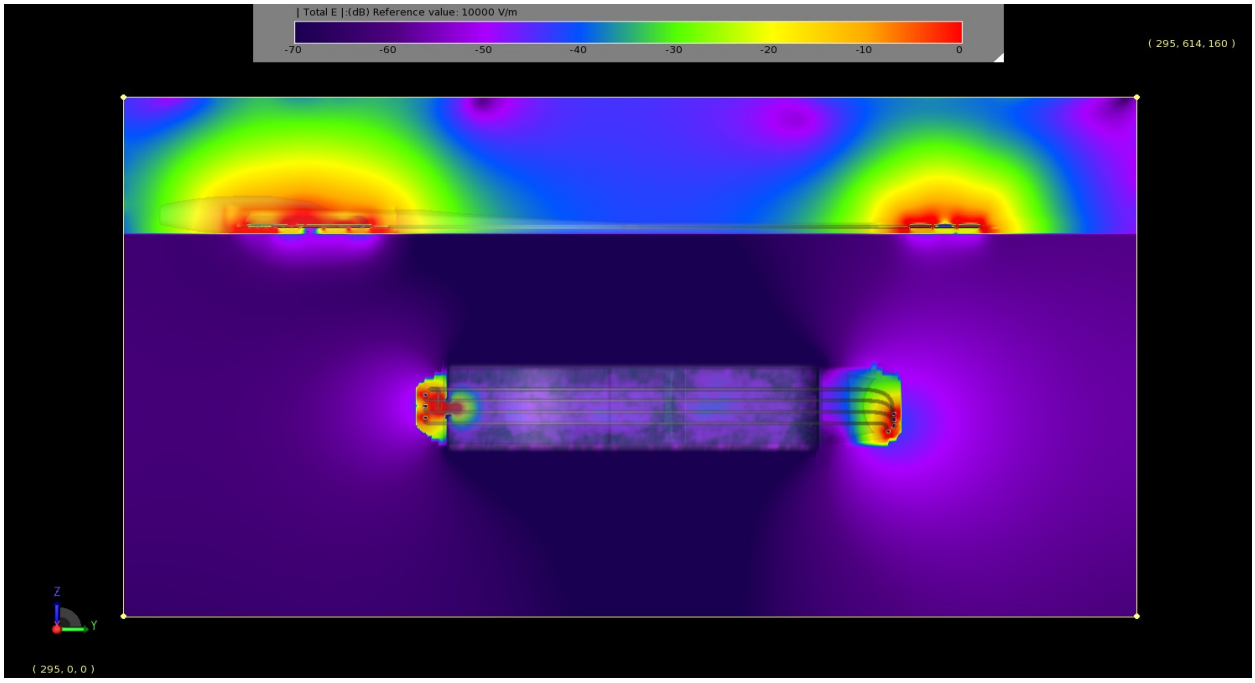

Illustration 34: Vertical slice computed E-field at 100 degrees phase. Normalized to 10,000 V/m.

5.1.5 Computed Power Dissipation Density

The simulation also provides computed power dissipation density (W/m^3). Power dissipation density is computed based on the conductivity of the materials and the square of the magnitude of the electric field. A plot of power dissipation density through the same vertical slice is shown in Illustration 35. Color scale is in dB and normalized to 1x10^8 W/m^3. Red regions can exceed normalization value. It is clear from this plot that the bulk of the power is dissipated not in the tissue, but in the IR losses of the coils and to a lesser extent in the losses of the titanium shell.

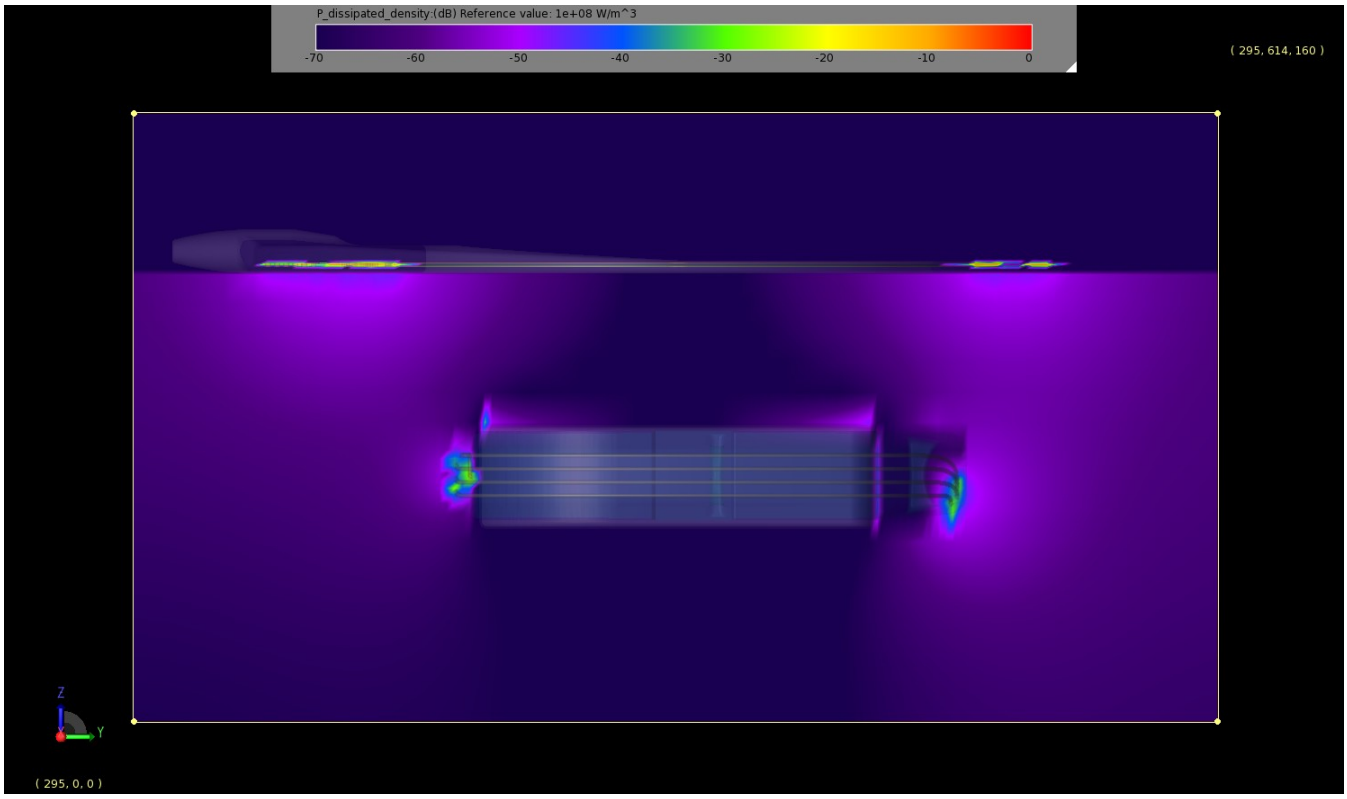

Illustration 35: Computed dissipated power density (W/m^3) vertical slice near center of simulation space

5.2 Offset Configuration

In this configuration, the RNR is shifted to the right approximately 24.2 mm. A top view of the CAD model for this case is shown in Illustration 36. This side view is identical to the centered configuration shown in Illustration 26.

As shown in the illustrations, the bottom surface of the transmit coil silicone covering is flush with the top face of the body phantom slab. The transmit coil is approximately centered laterally in the solution space. Excepting the silicone region forming the coaxial feed cable stress relief, the shortest distance from the edge of the transmit coil covering to a boundary face is approximately 27 mm.

The top face of the RNR is located approximately 25 mm below the top face of the body phantom. This is the recommended implant depth for the device. The bottom face of the RNR device is thus located approximately 33 mm above the bottom face of the body phantom slab. The RNR is offset from lateral center and the shortest lateral distance from a side face of the RNR device to the boundary of the body phantom is approximately 31 mm.

Again, the above mentioned distances to boundaries do NOT include PML (Perfectly Matched Layers).

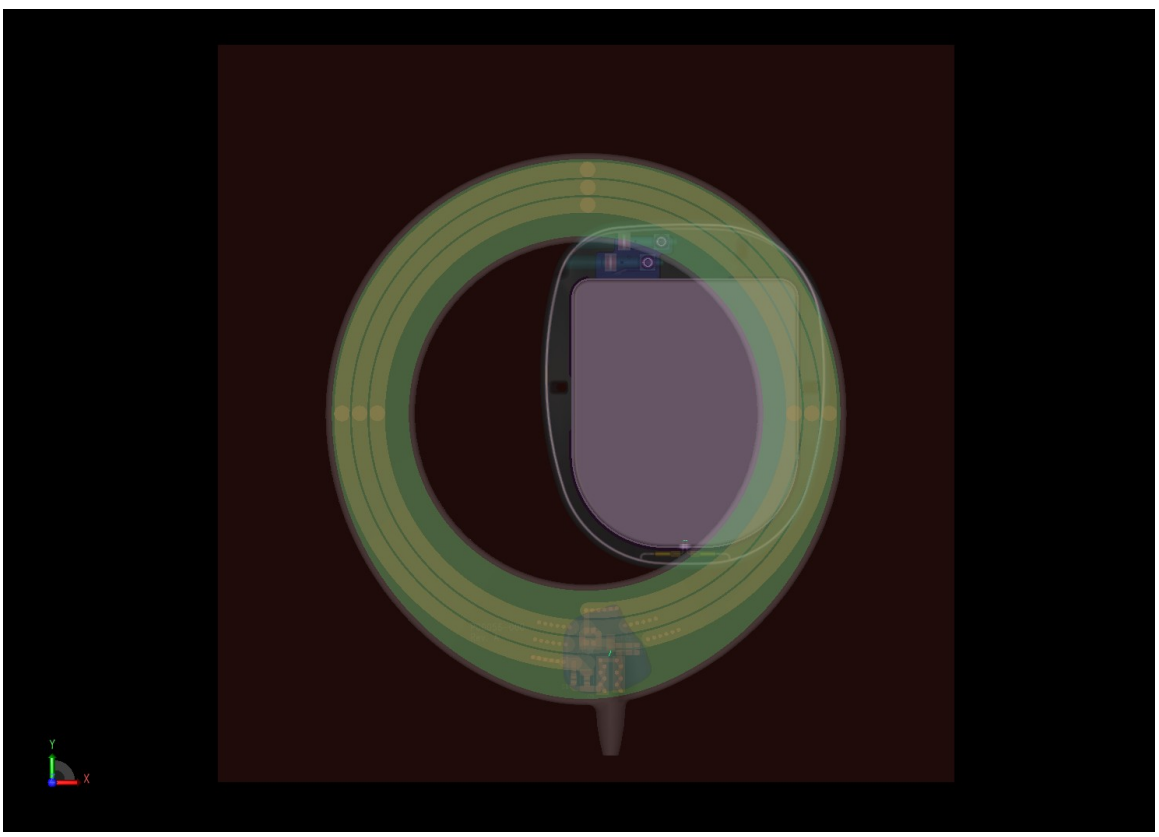

Illustration 36: Top view of offset configuration.

5.2.1 Simulation Diagnostics

The Remcom simulator was configured to run a minimum of two and a maximum of four oscillations of the 6.78 MHz sinusoid. The workstation was configured to run using all available cores (1792 CUDA cores and 8 CPU cores) and required approximately 31 hours to compute the steady state fields. The solution reached a convergence value of -35.01 dB which is generally considered an acceptable for a steady state solution. An additional 9.25 hours was required to compute the 1 gram and 10 gram SAR averages.

5.2.2 Computed Current and Voltage Waveforms

As shown in the previous section, the source condition for the TC is 1117.2 mA peak at 0 degrees phase. The source condition for the RNR is 875.4 mA peak at -100 degrees phase.

A plot of computed current through the TC and RNR source is shown in Illustration 37. The TC curve (blue) is sinusoidal and peaks at approximately 1020.6 mA. This is approximately 8.6% low as compared to the source condition. This deviation is likely the result of differences between the TC and RNR coupling in the measurement versus simulation. The RNR curve (red) exhibits a slight turn on transient in the initial ½ cycle and is sinusoidal thereafter. The peak values are approximately 875mA which is very close to the 875.4mA source value.

A plot of the computed voltage at the TC and RNR coil terminals is shown in Illustration 38. The TC voltage (blue) exhibits a turn on transient but becomes sinusoidal after approximately 1 cycle. The peak voltage is approximately 103.5V. The RNR coil voltage also exhibits a turn on transient which dies out with approximately 1 cycle and is sinusoidal thereafter. The peak of the sinusoids is approximately 62.2V. Both voltage waveforms are consistent with the expected device operation.

The Remcom solver was configured to record only steady state fields (as opposed to transient fields) so the effects of the transient currents and voltages shown above are not included in the field plots or SAR calculations shown in the next section.

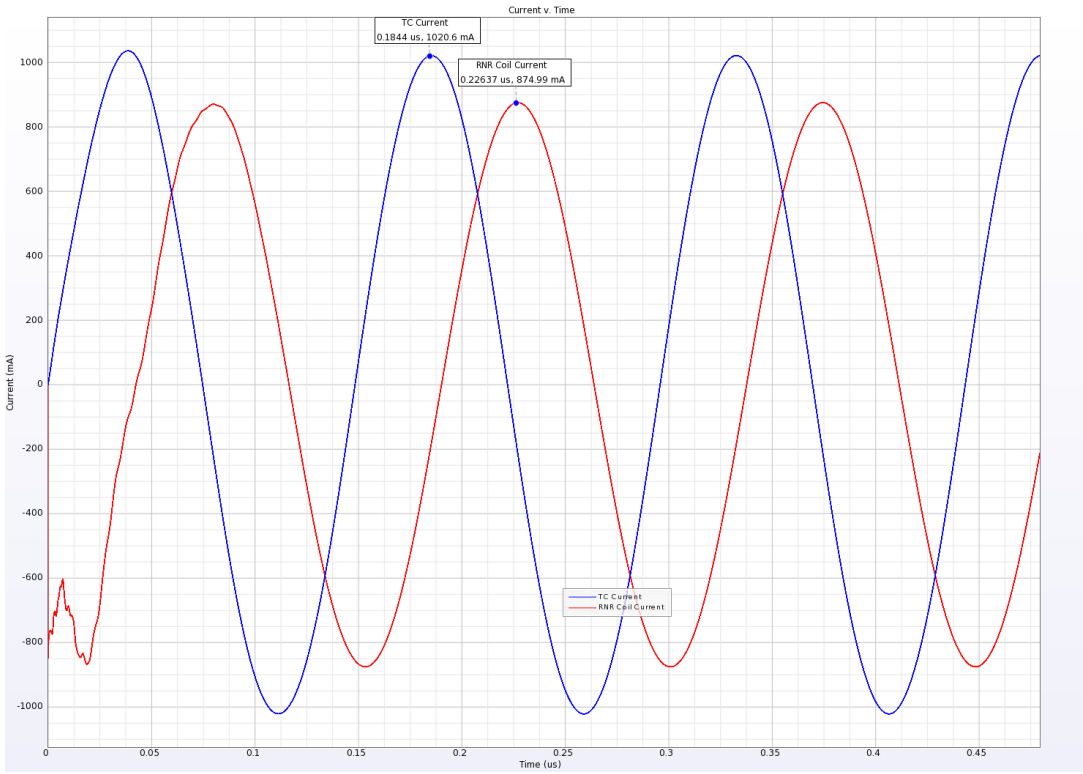

Illustration 37: Computed current waveform in TC and RNR coil.

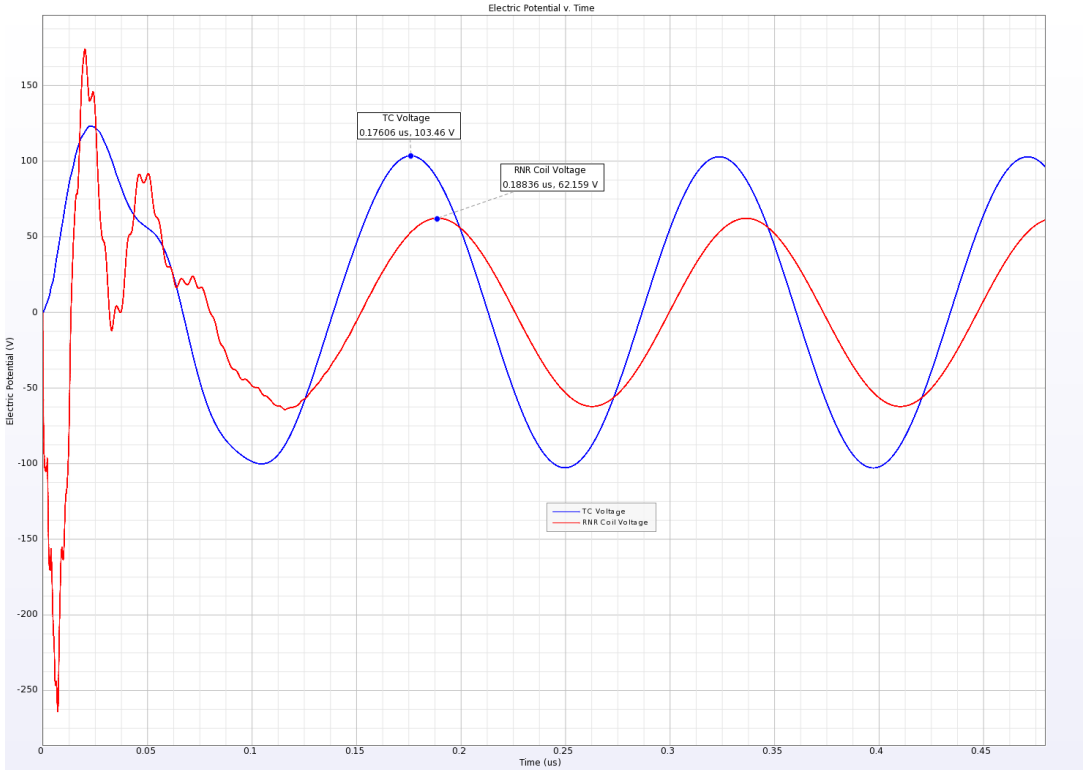

Illustration 38: Computed voltages on TC and RNR

5.2.3 Computed B-fields

Centered Probe on TC

A plot of the z-component of computed B-field (uT) in a horizontal slice taken just above (+1mm) the plane of the TC is shown in Illustration 39. Color scale is linear and normalized to 50uT. Red regions can exceed normalization value. Phase angle is 105 degrees. The B-field at the pointer location is ~36.7uT peak (25.9uT RMS). Field gradient is clearly small in this region so probe averaging effects should be minimal.

Centered Probe between TC and RNR

A plot of the z-component of computed B-field (uT) in a horizontal slice taken midway between the TC and RNR (z=-12.7358mm) is shown in Illustration 40. Color scale is linear and normalized to 50uT. Red regions can exceed normalization value. Phase angle is 110 degrees. The B-field at the pointer location is ~27.6uT peak (19.5uT RMS). Field gradient is more pronounced in this case as compared to the centered case due to RNR offset. Probe averaging effects will skew data somewhat compared to single point values in the simulation.

Comparison to Measurement

A summary of the the B-field probe measurements and B-field computations is shown in Table 15. Measured values represent the average of data taken when testing the TC and RNR coil. Computations are peak values near center of probe location and do not account for probe averaging. The agreement is reasonable.

Location	Measured B-field (uT)	Computed B-field (uT)
TC centered, z=+1mm	24.15	25.9
TC centered, z=-12.7mm	20.15	19.5

Table 15: Measured versus computed B-field for offset configuration.

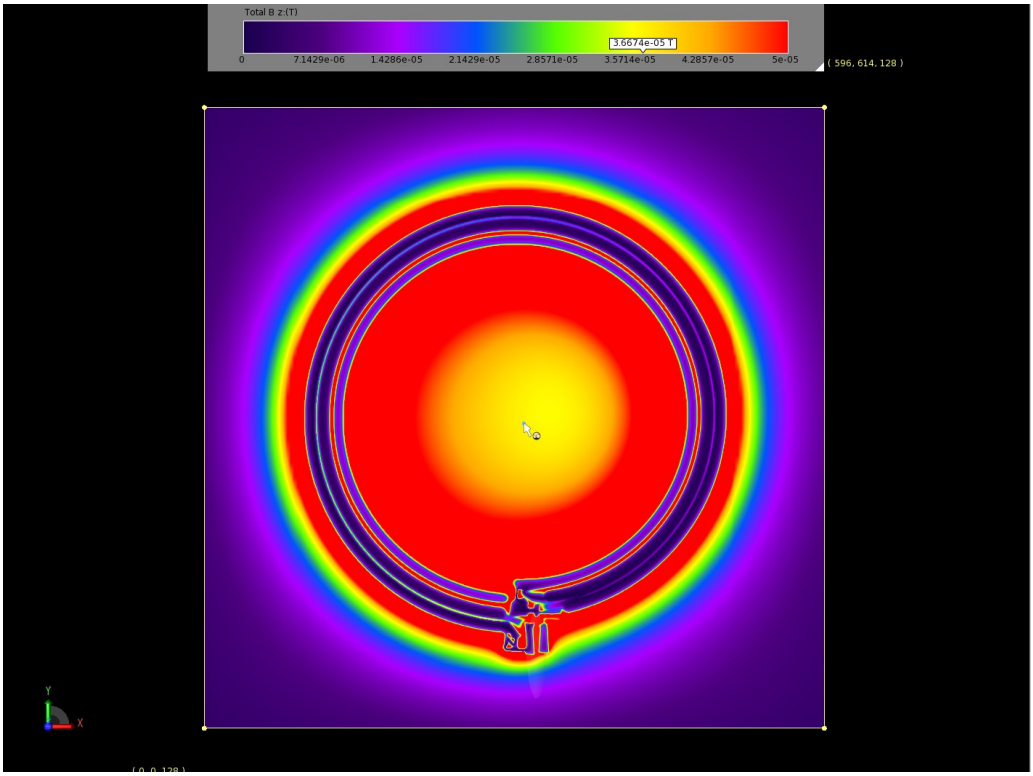

Illustration 39: Offset configuration B-field slice in plane of TC.

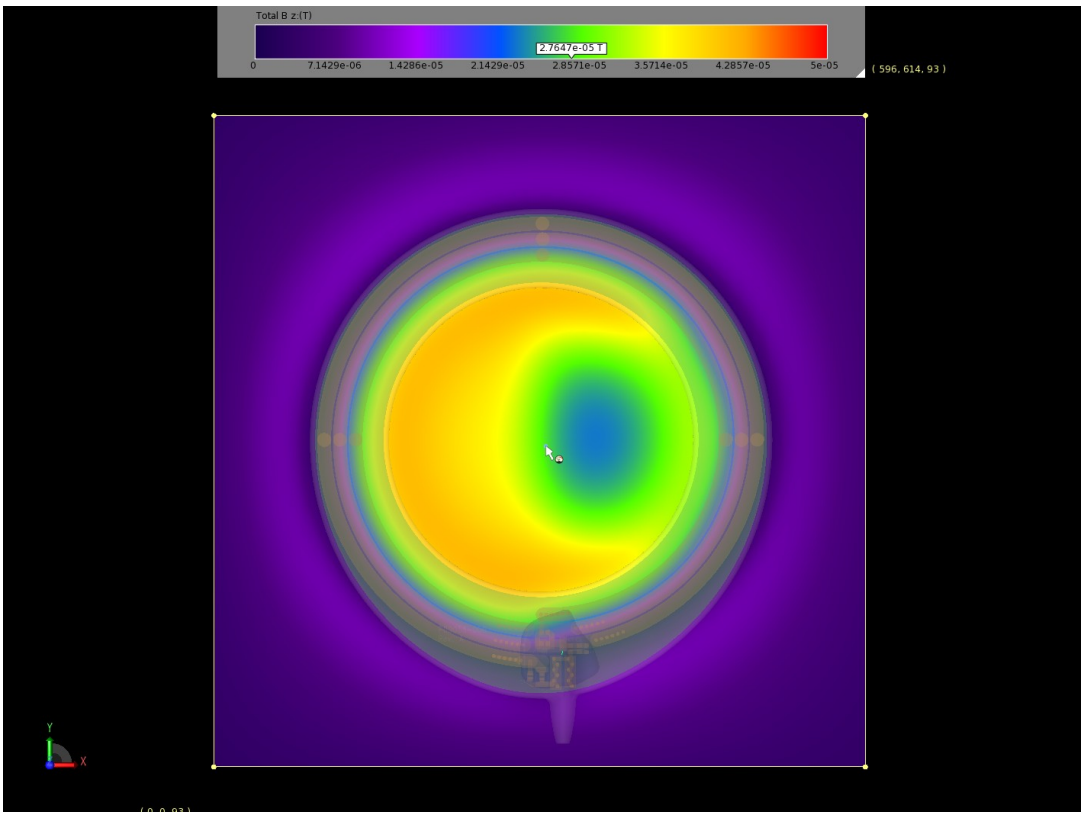

Illustration 40: Offset configuration B-field slice midway between TC and RNR.

5.2.4 Additional H-Field and E-Field plots

A false color plot of the computed H-field (A/m) in a vertical slice taken through the approximate center of the simulation space is shown in Illustration 41. Color scale is in dB and normalized to 1000 A/m. Red regions can exceed normalization value. This particular image is for 0 phase and shows weak H-fields near the TC and stronger fields near the RNR coil. The plot of Illustration 42 (same scale) shows the same vertical slice at 100 degree phase angle. Here, the fields are much stronger near the TC and weaker near the RNR coil. Both of these plots are consistent with the -100 degree phase angle difference used in the excitation on each coil.

A false color plot of the computed E-field (V/m) in the same vertical slice is shown in Illustration 43. Color scale is in dB and normalized to 10,000 V/m. Red regions can exceed normalization value. The zero phase plot shows that the E-field levels are maximum inside the TC and near the windings of the RNR coil. Maximum field values are reached in non-tissue media. The fields decay extremely rapidly with distance from the transmit and RNR coils. Field values in most of the tissue region are many orders of magnitude lower than values computed in the tissue phantom. The plot for 100 degree phase is shown in Illustration 44 (same scale) and again shows that peak values are generally limited to non-tissue regions and that they decay very rapidly with distance.

It should be noted that there E and H field plots do not show any indication of extraneous reflections from the absorbing boundary layers imposed on the tissue slab surfaces (not including top where the coil is placed). This efficiency of the absorbing boundary condition is critical to ensure the validity of the FDTD solution.

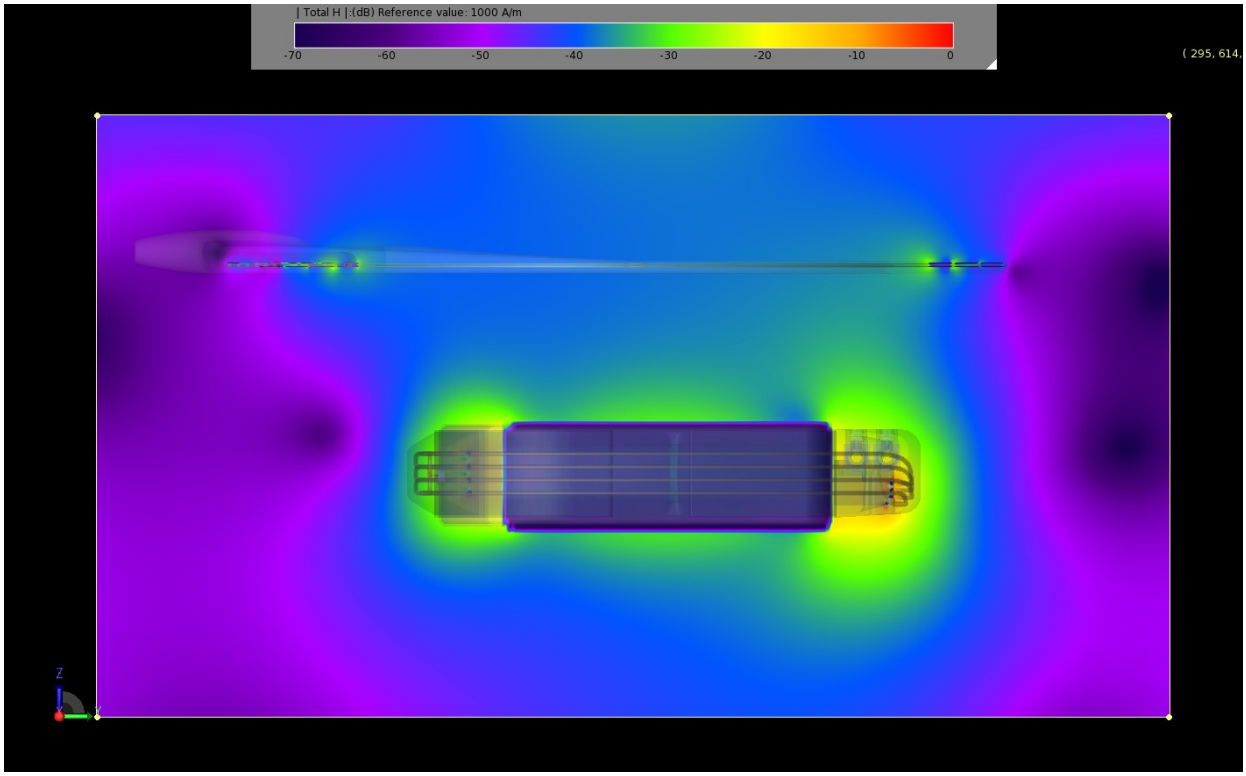

Illustration 41: Computed H-Field at 0 degrees phase. Vertical slice. Normalized to 1,000 A/m.

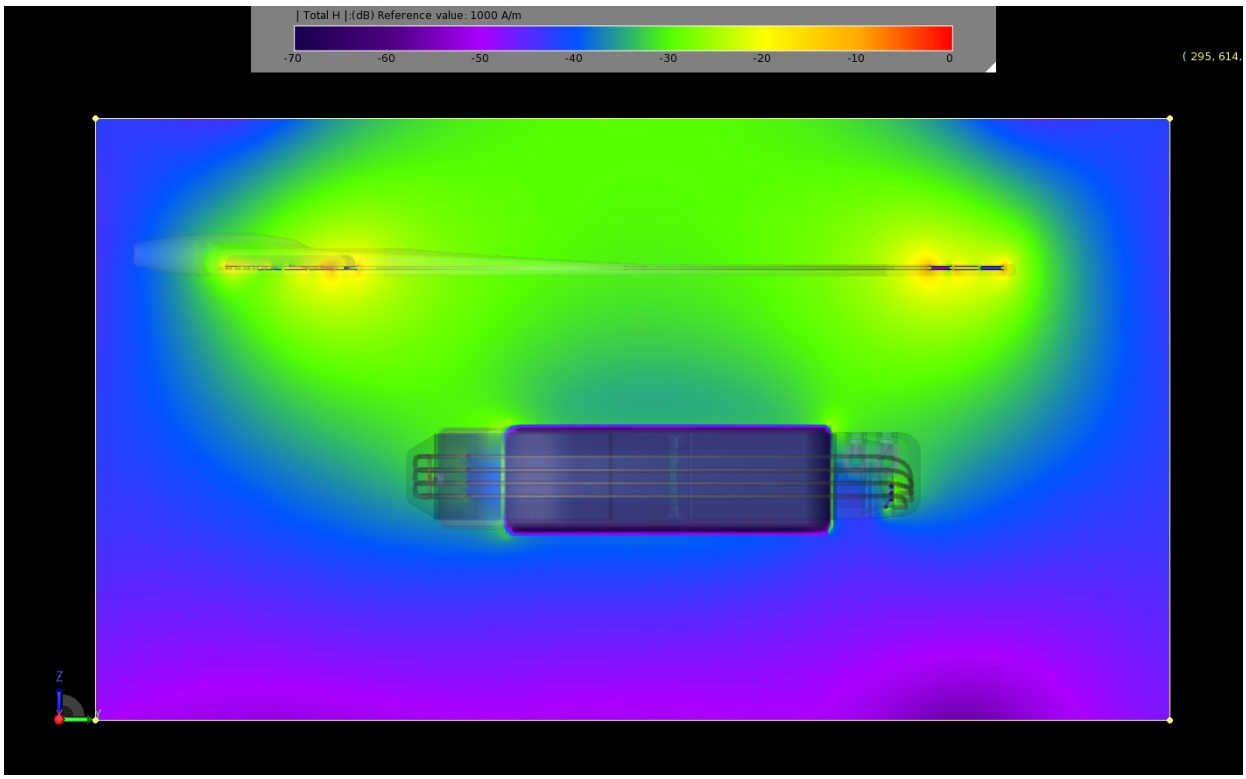

Illustration 42: Computed H-Field at 100 degrees phase. Vertical slice. Normalized to 1,000 A/m.

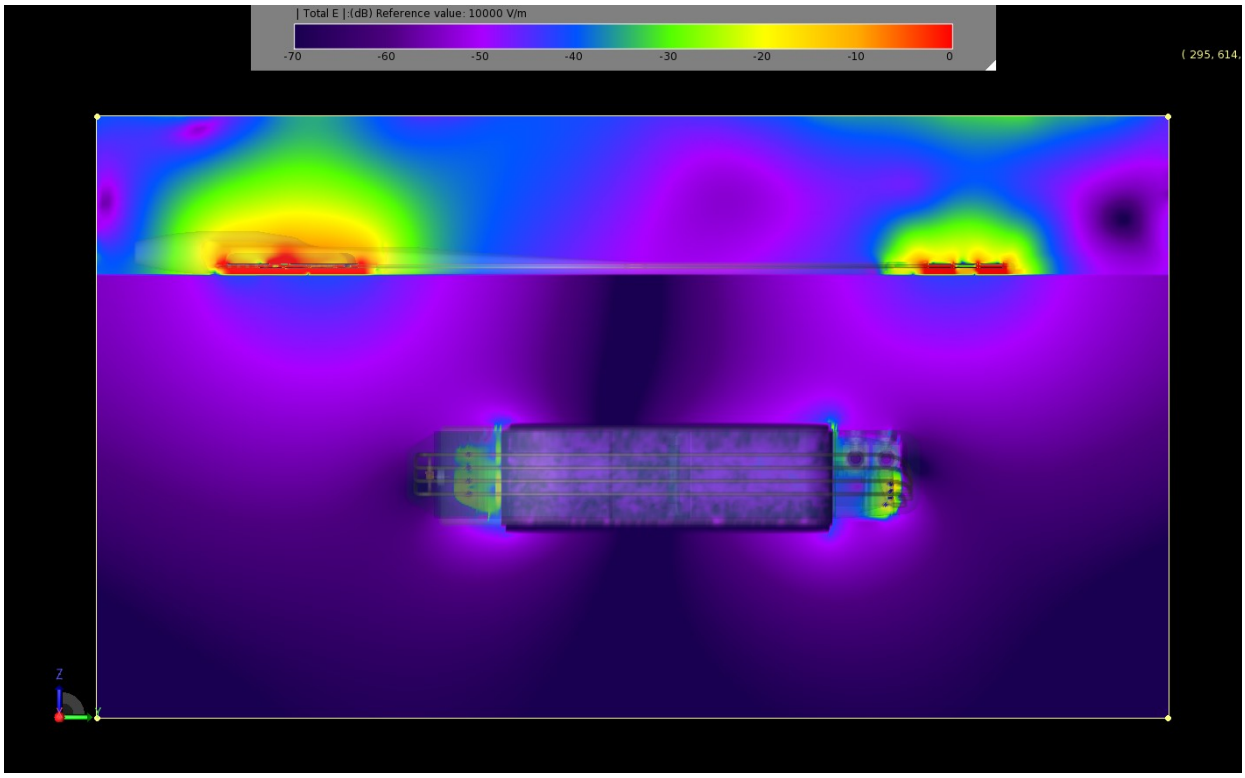

Illustration 43: Computed E-field at 0 degrees phase. Vertical slice. Normalized to 10,000 V/m.

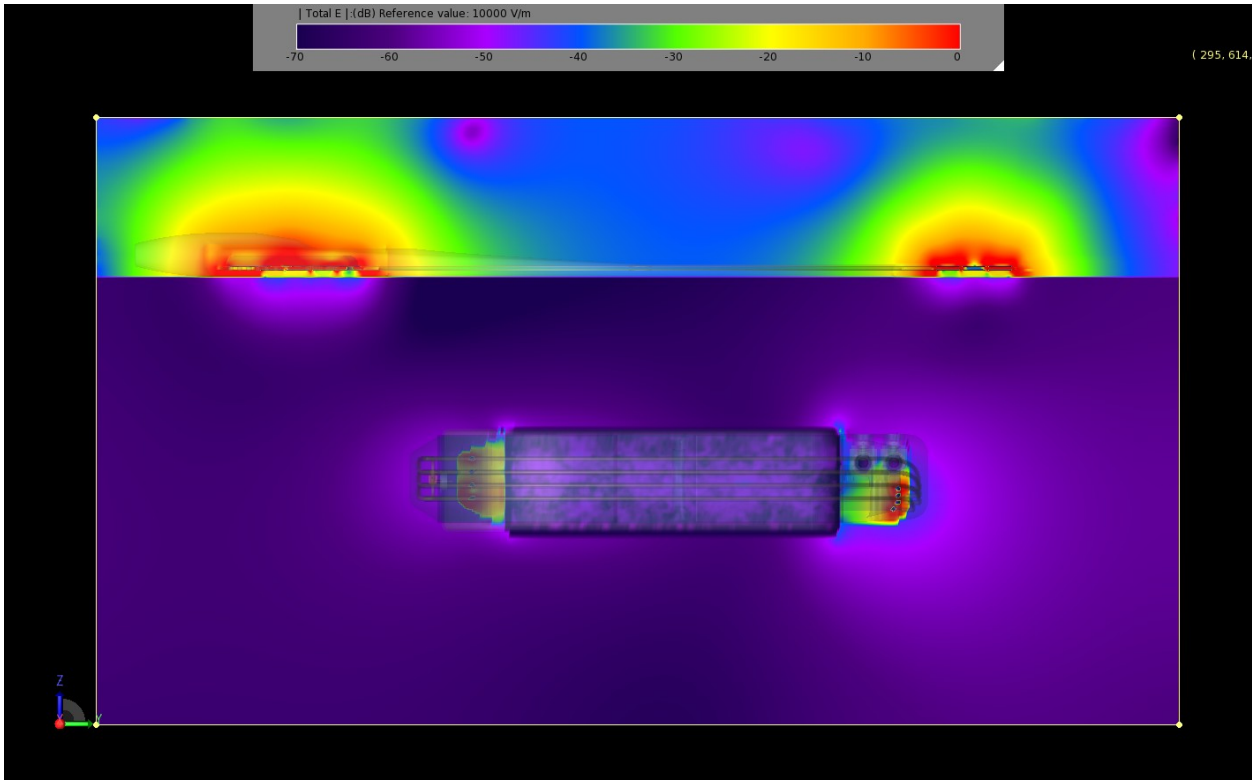

Illustration 44: Computed E-field 100 degrees phase. Vertical slice. Normalized to 10,000 V/m.

5.2.5 Computed Power Dissipation Density

The simulation also provides computed power dissipation density (W/m^3). Power dissipation density is computed based on the conductivity of the materials and the square of the magnitude of the electric field. A plot of power dissipation density through the same vertical slice is shown in Illustration 45. Color scale is in dB and normalized to 1x10^8 W/m^3. Red regions can exceed normalization value. It is clear from this plot that the bulk of the power is dissipated not in the tissue, but in the IR losses of the coils and to a lesser extent in the losses of the titanium shell.

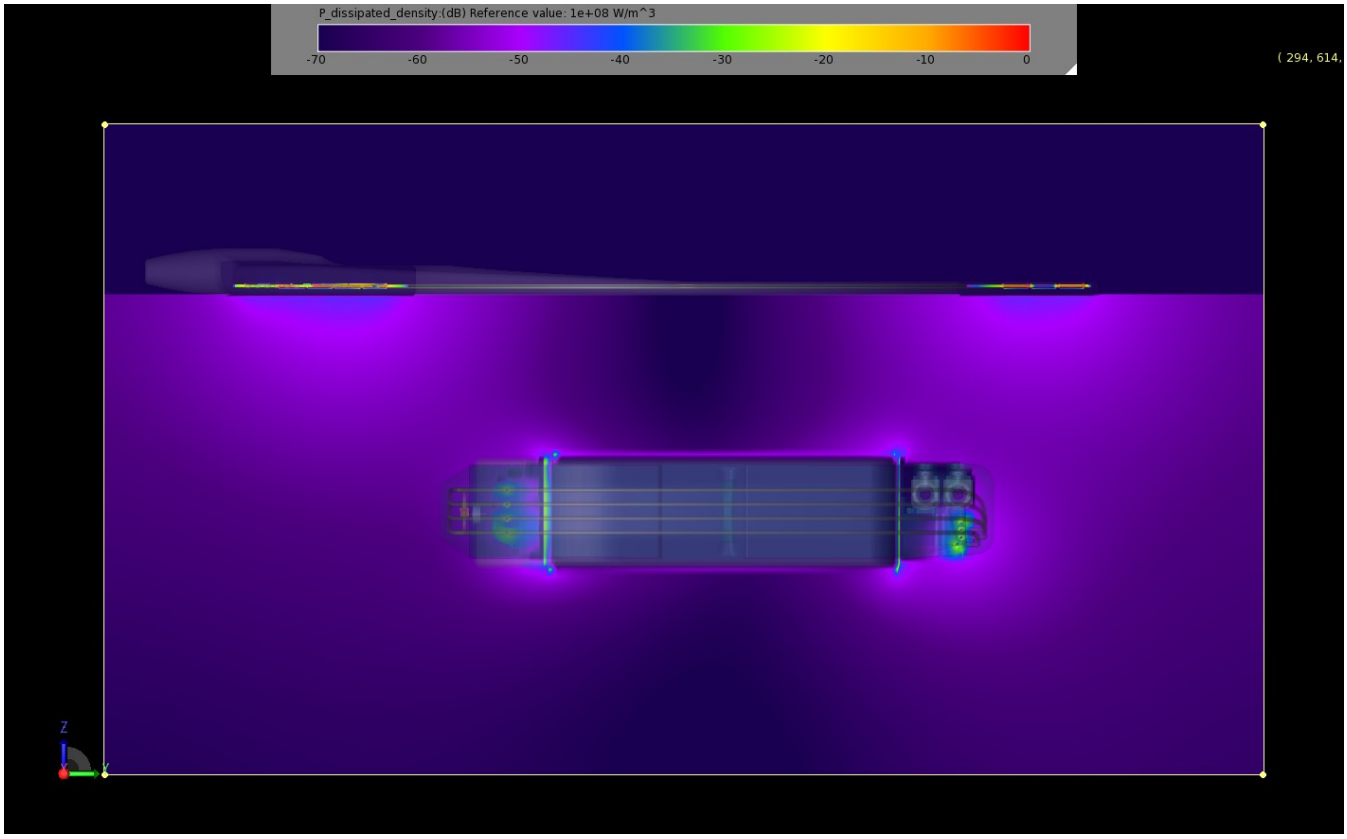

Illustration 45: Computed dissipated power density (W/m^3) vertical slice near center of simulation space

6 SAR Analysis

The previous section demonstrated the validity of the field values computed by the simulator. This section examines the SAR values that are computed based on the EM field values and assumed material properties.

6.1 Centered Configuration

6.1.1 Computed SAR Results

The simulator computed 1 gram and 10 gram SAR averages. Computations were limited to regions inside the tissue slab and do not include regions where the averaging calculations would include non-tissue regions.

The computed maximum 1 gram SAR average value was 0.9039 W/kg.

A vertical slice containing the maximum SAR value for the 1 gram calculation is shown in Illustration 46. Color scale is linear and normalized to 0.9039 W/kg. Red regions can not exceed normalization value. The peak SAR levels are reached in the region of the directly under the feed region of the TC.

A horizontal slice containing the maximum 1 gram SAR average value is located 1.56 mm below the air-body phantom interface, which is as close to the air-phantom boundary as allowed by the simulator. A false color plot for that slice is shown in Illustration 47 (same scale).

The computed maximum 10 gram SAR average was 0.4896 W/kg.

A vertical slice containing the maximum SAR value for the 10 gram calculation is shown in Illustration 48. Color scale is linear and normalized to 0.4896 W/kg. Red regions can not exceed normalization value. The maximum values are reached just below the TC. There is some distortion of the curves due to the required averaging process.

A horizontal plane slice containing the maximum SAR value for the 10 gram calculation is shown in Illustration 49 (same scale). Again, the slice is taken 1.5mm below the air-phantom interface, which is as close to the air-phantom boundary as allowed by the simulator.

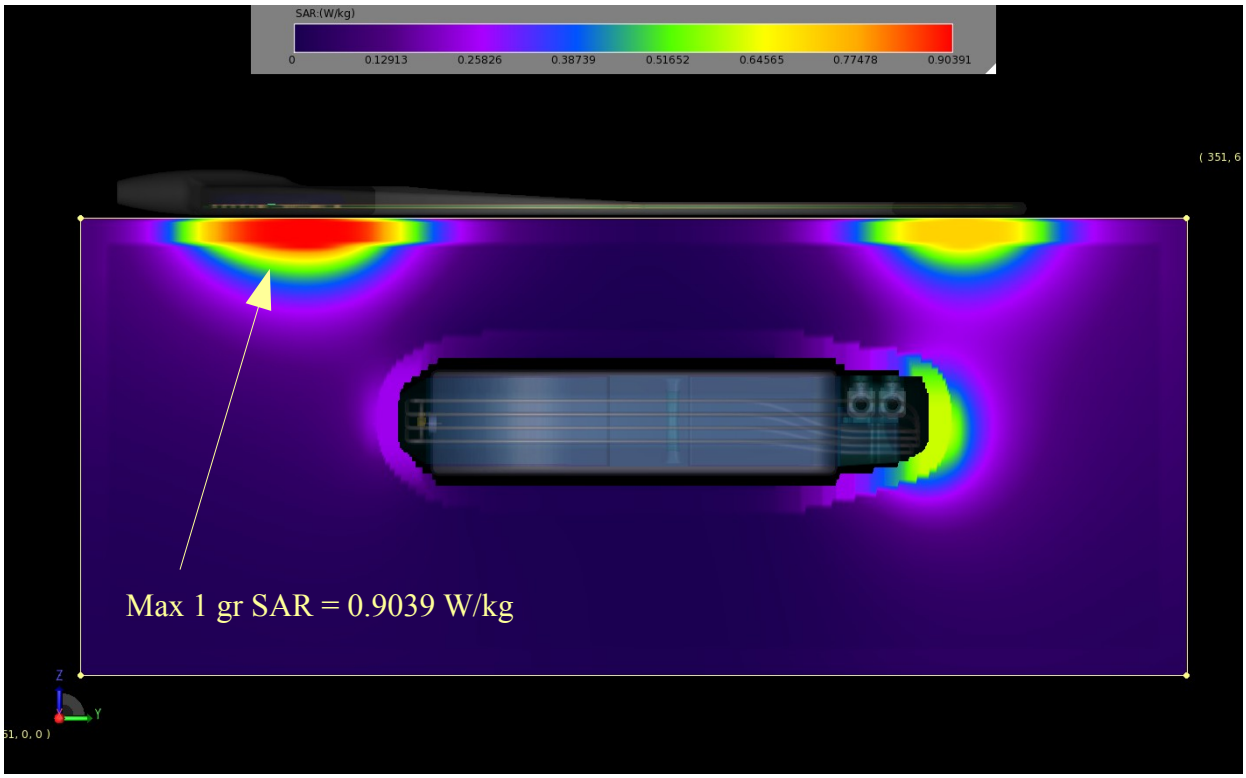

Illustration 46: Vertical slice containing maximum 1 gr SAR.

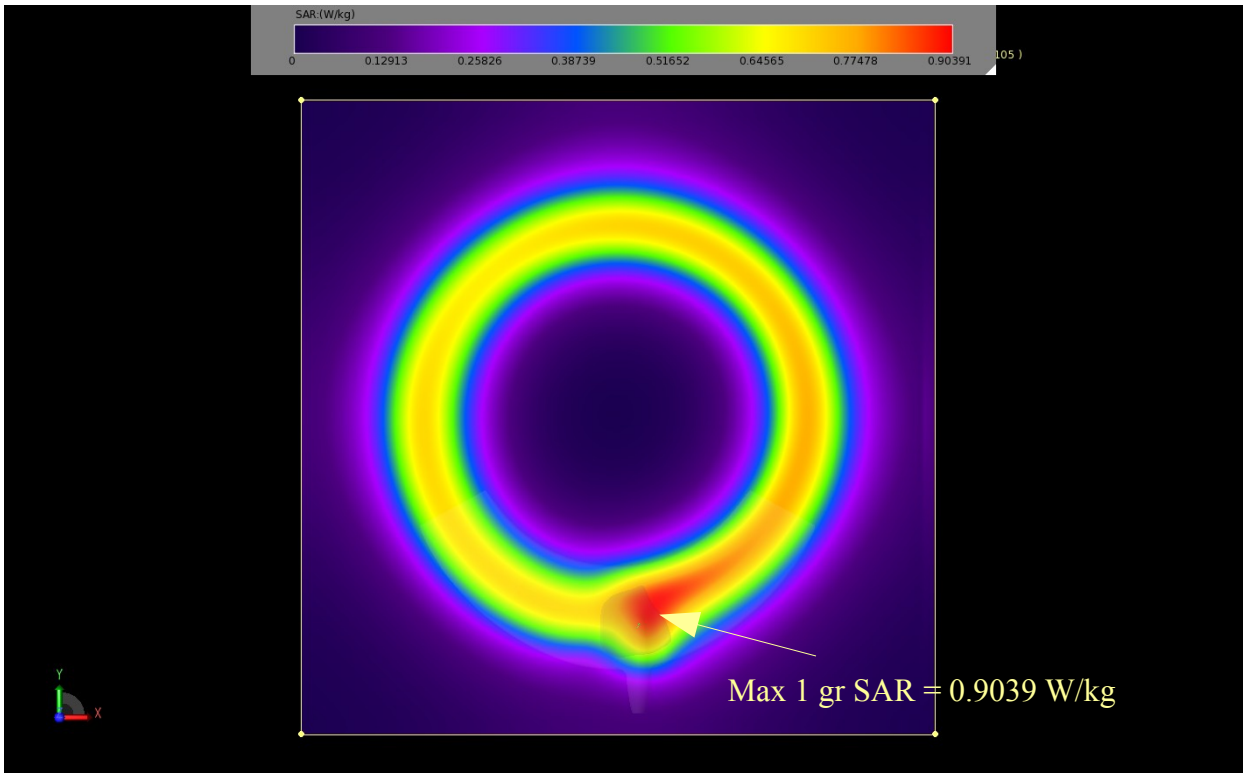

Illustration 47: Horizontal slice containing maximum 1 gr SAR.

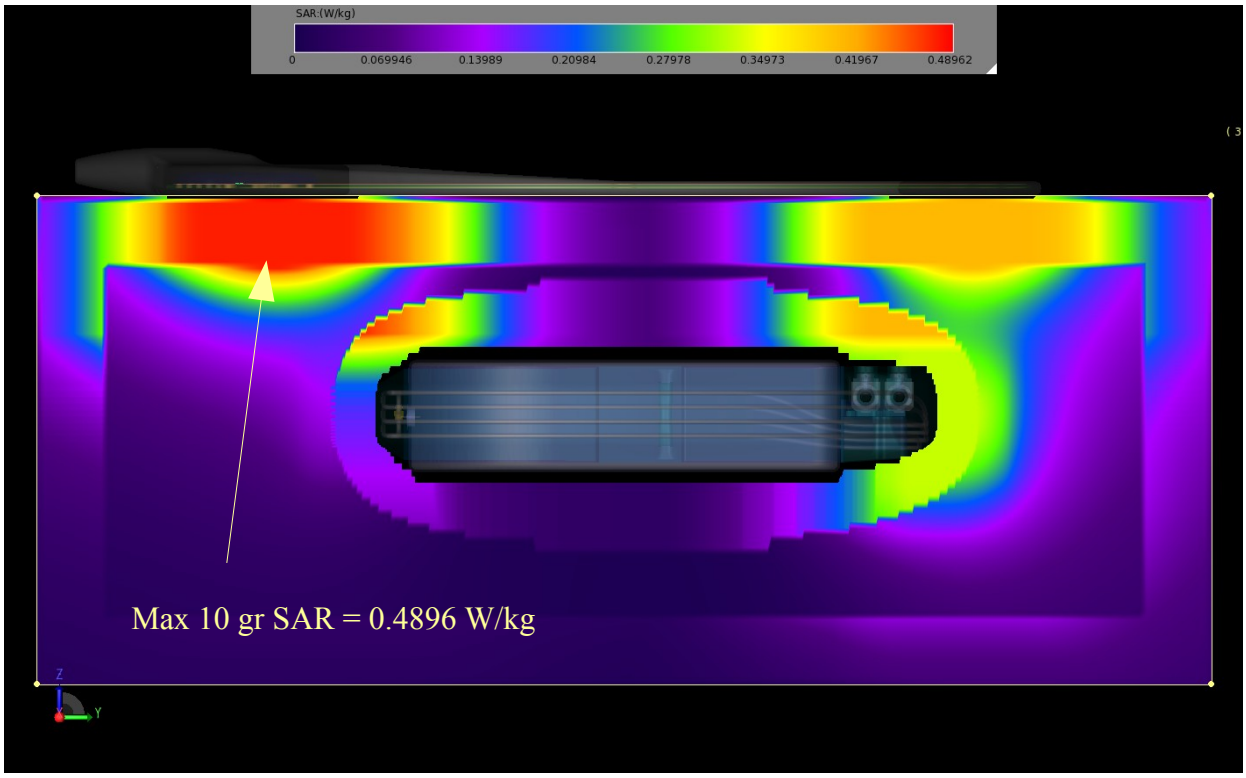

Illustration 48: Vertical slice containing maximum 10 gr SAR.

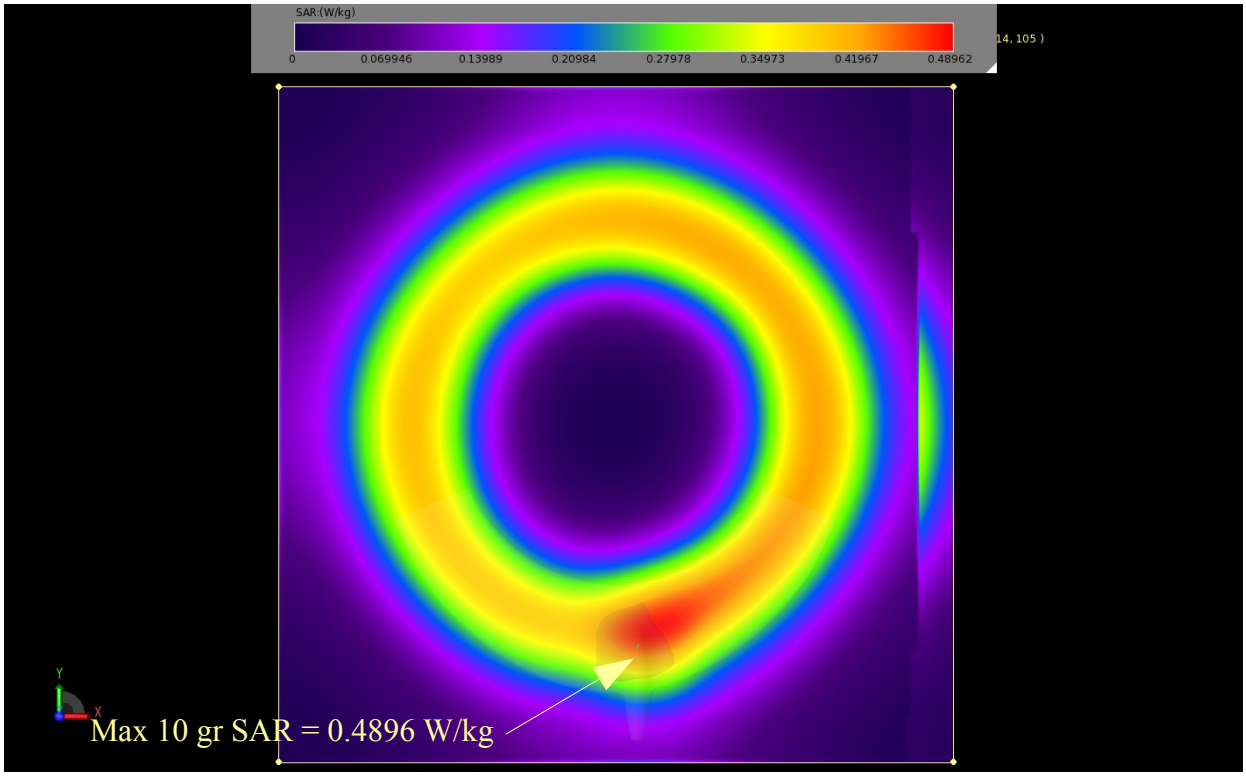

Illustration 49: Horizontal slice containing maximum 10 gr SAR.

6.2 Offset Configuration

The simulator computed 1 gram and 10 gram SAR averages. Computations were limited to regions inside the tissue slab and do not include regions where the averaging calculations would include non-tissue regions.

The computed maximum 1 gram SAR average value was 1.3842 W/kg.

A vertical slice containing the maximum SAR value for the 1 gram calculation is shown in Illustration 50. Color scale is linear and normalized to 1.3842 W/kg. Red regions can not exceed normalization value. The peak SAR levels are reached in the region of the directly under the feed region of the TC.

The horizontal slice containing the maximum 1 gram SAR average value is located 1.56 mm below the air-body phantom interface, which is as close to the air-phantom interface as allowed by the simulator. A false color plot for that slice is shown in Illustration 51 (same scale).

The computed maximum 10 gram SAR average was 0.7582 W/kg.

A vertical slice containing the maximum SAR value for the 10 gram calculation is shown in Illustration 52. Color scale is linear and normalized to 0.7582 W/kg. Red regions can not exceed normalization value. The maximum values are reached just below the TC. There is some distortion of the curves due to the required averaging process.

A horizontal plane slice containing the maximum SAR value for the 10 gram calculation is shown in Illustration 53 (same scale). The horizontal slice is taken 1.56 mm below the air-phantom interface, which is as close to the air-phantom interface as allowed by the simulator.

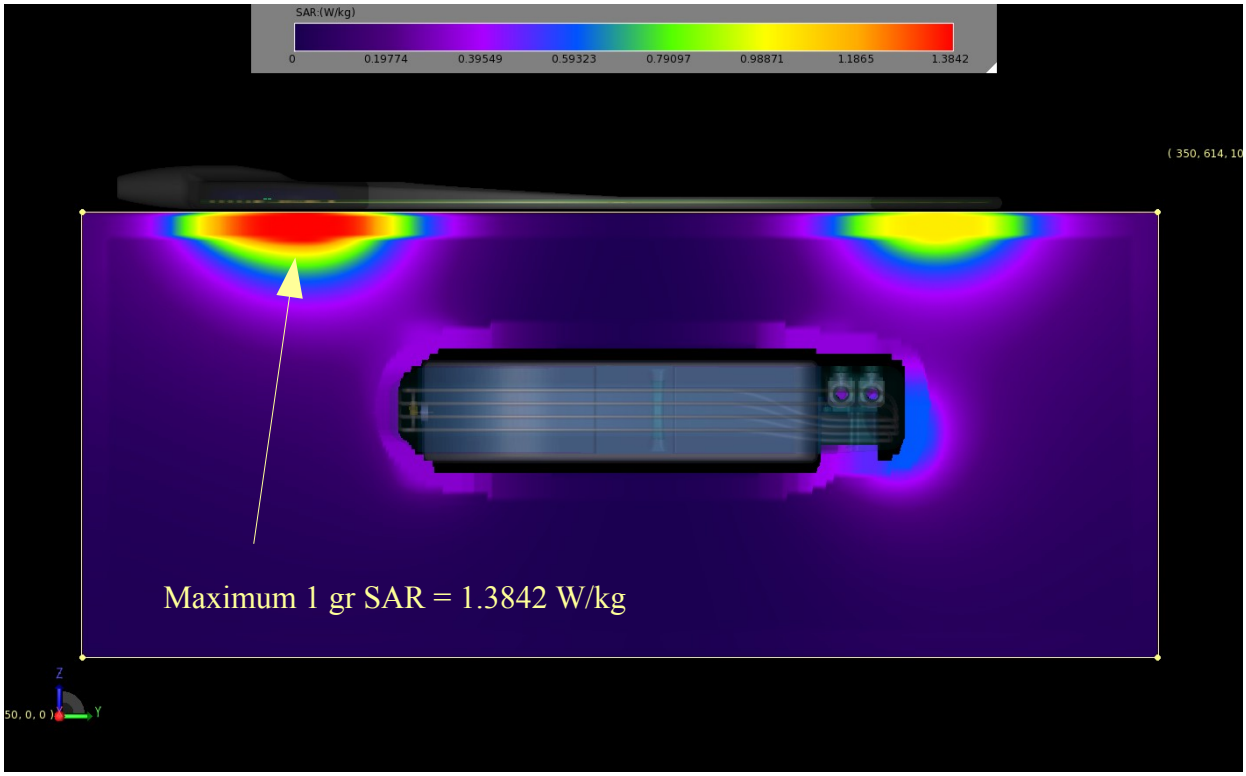

Illustration 50: Vertical slice containing maximum 1 gr SAR.

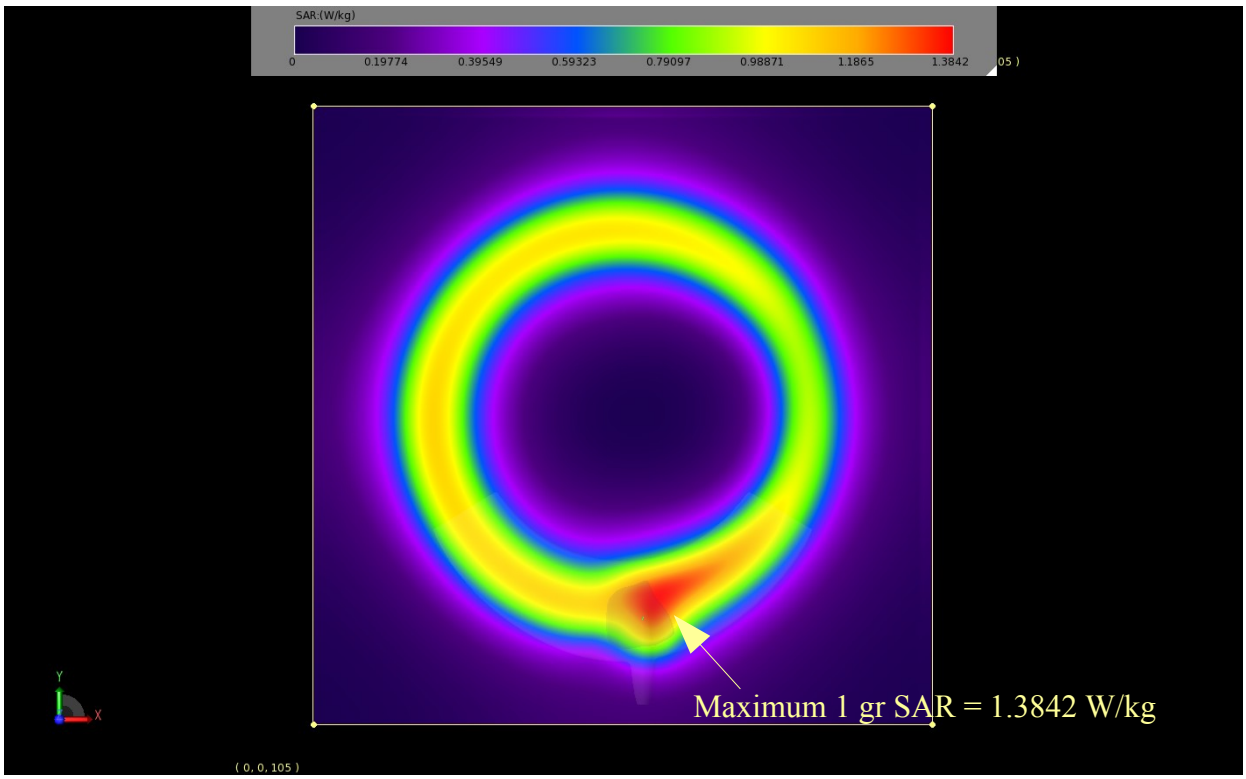

Illustration 51: Computed 1 gram SAR average in horizontal max slice 1.56 mm below TC.

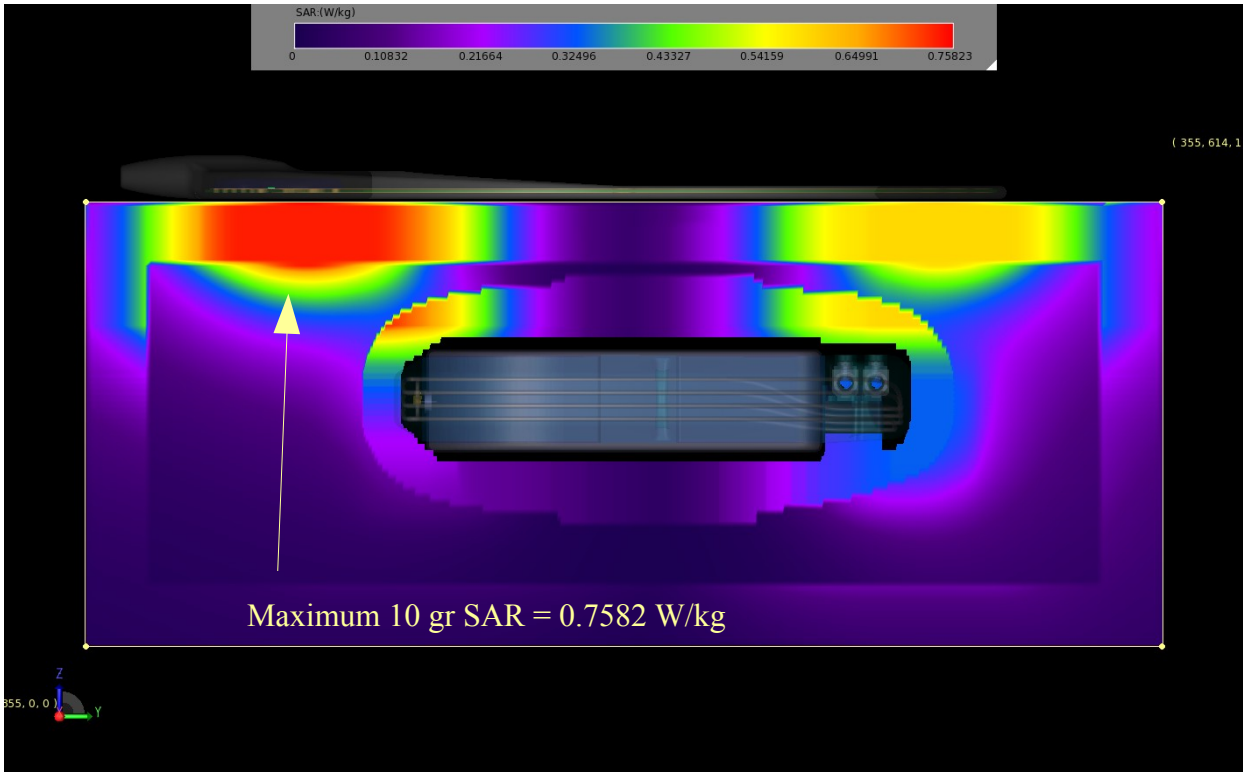

Illustration 52: Vertical slice containing maximum 10 gr SAR.

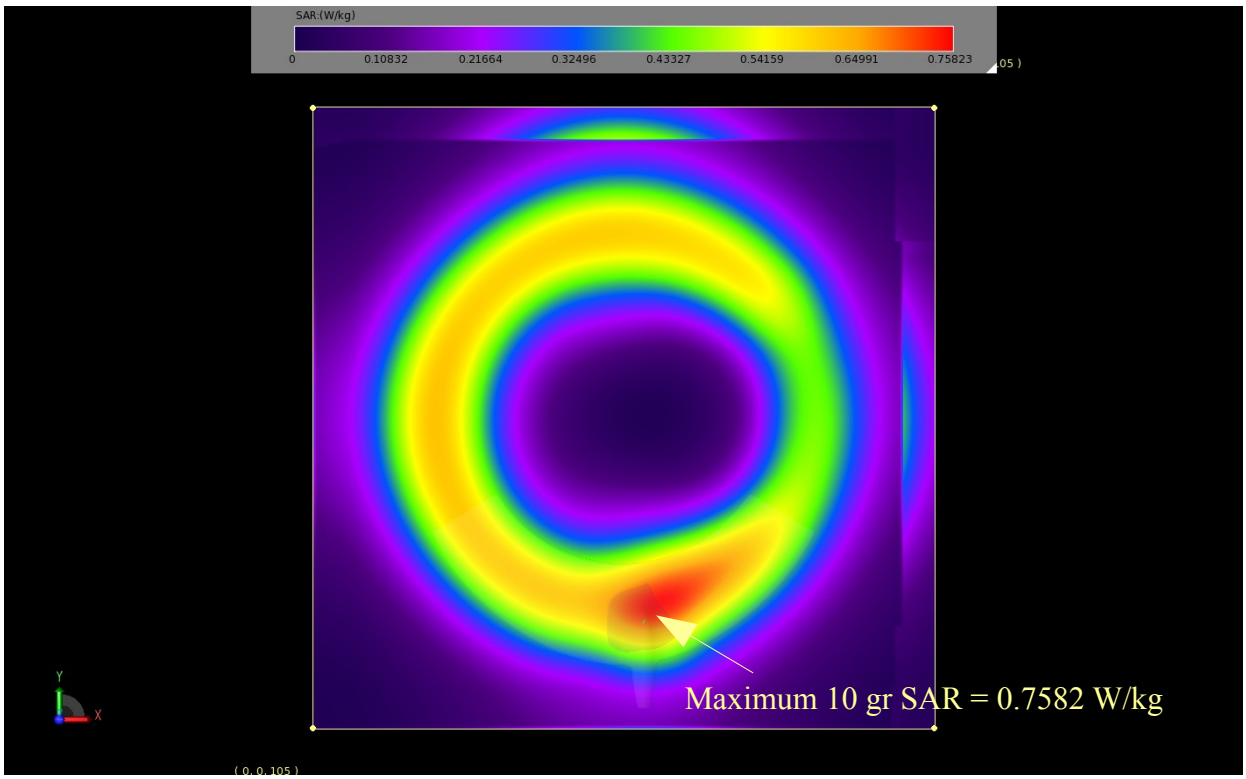

Illustration 53: Horizontal slice containing maximum 10 gr SAR.

6.3 FCC SAR Requirements

The FCC regulations for SAR limits for General Population / Uncontrolled Exposure Limits are summarized in Table 16. These values are the most restrictive of the exposure rules imposed by the FCC. The Whole Body SAR is to be averaged over the entire body. The Partial-Body SAR is averaged over any 1 gram of tissue in the shape of a cube. SAR for hands, wrists, feet and ankles is averaged over any 10 g of tissue in the shape of a cube.

Whole-Body	Partial-Body	Hands, Wrists, Feet and Ankles
0.08	**1.6**	**4.0**

Table 16: General Population/Uncontrolled Exposure Limits (W/kg)

The calculations of the previous sections have shown that that the worst case / offset configuration produces a maximum computed 1 gram SAR average of 1.3842 W/kg. The nominal / centered configuration produces a maximum 1 gram SAR average of 0.9039 W/kg. Both values are below the 1.6 W/kg value set by the FCC for Partial-Body SAR (1 gram average) for General Population / Uncontrolled Exposure Limits.

The calculations of the previous sections have also shown that the worst case / offset configuration produces a maximum computed 10 gram SAR average of 0.7582 W/kg. The nominal / centered configuration produces a maximum 10 gram SAR average of 0.4896 W/kg. Again, both figures are well below the 4.0 W/kg value set by the FCC for Hands, Wrists, Feet and Ankles for General Population / Uncontrolled Exposure Limits.

Lastly, there is the issue of Whole-Body SAR. With the device in question it is impractical to consider modeling the whole body SAR using a FDTD code and a human voxel model. That said, worst case / offset configuration produced an average SAR over the entire 2.336 kg of tissue phantom of 0.1174 W/kg. The nominal / centered configuration was even lower at 0.08494 W/kg. Since the regions with significant SAR exposure are limited to the regions very near the device, taking the average over a larger body will only reduce the SAR value. The EnteroMedics device is intended to treat obesity in adult humans whose body mass is significantly larger than the small tissue phantom used here. It therefore seem reasonable to argue that Whole-Body requirement will be met in all normal use cases.

7 Summary

A SAR analysis of the EnteroMedics Inc. Maestro Rechargeable System has been completed and demonstrates that it meets the FCC General Population / Uncontrolled Exposure Limits.

The SAR simulation required use of a novel approach of mixing a Spice based circuit simulation with measured data to jump start a steady state FDTD electromagnetic field simulation. Using this approach, the computed current waveforms track reasonably well with the expected / measured values of the device. In the case of the TC, current is within ~10% of the expected value. The RNR coil agreement is significantly better. The voltages computed at the terminals of the TC and the RNR coil are within expectation as modeled. Predicted B-field values correlate well with measured B-field data in regions where field gradient is modest.

8 Statement of Compliance

The maximum results of the Specific Absorption Rate (SAR) found through computational modeling of the **EnteroMedics Inc. Maestro Rechargeable System** are shown in Table 17 below. Values were computed with the Transmit Coil at zero distance from a homogeneous body slab model and the RNR unit 2.5 cm (recommended spacing) below the air to homogeneous body phantom model interface.

SAR Calculation Type	Partial-Body (1 gr Average)	Hands, Wrists, Feet and Ankles (10 gr Average)
Maximum Computed Value (W/kg)	**1.3842**	**0.7582**

Table 17: Maximum computed SAR values.

It has therefore been demonstrated through a computational modeling approach that the EnteroMedics Inc. Maestro Rechargeable System has Specific Absorption Rate (SAR) that is in compliance with the FCC General Population/Uncontrolled exposure Limits specified in FCC 47 CFR part 2 (2.1093) and ANSI/IEEE C95.1-1992.